Unsteadiness of an axisymmetric separating-reattaching flow

Sebastien Deck* and Pascal Thorigny

ONERA, Applied Aerodynamics Department,

29 av. de la Division Leclerc, 92322 Châtillon Cedex, FRANCE

(Dated: January 15, 2007)

Abstract

The separated flow behind an axisymmetric step at high subsonic regime is investigated numerically and compared with the experimental data of Deprés *et al.*[1]. Firstly, it is shown that this axisymmetric step flow has much in common with the two-dimensional facing step flows as regards the shear layer instability process. Secondly, the statistical and spectral properties of the pressure fluctuations are scrutinized. Close to the step, the surface pressure signature is characterized by low frequencies $f.L_r/U_\infty = \mathcal{O}(0.08)$ and an upstream velocity of $0.26U_\infty$ while in the second half-part of the recirculation higher frequencies fluctuations at $f.L_r/U_\infty \approx 0.6$ and a downstream convection velocity $0.6U_\infty$ are the dominant features. The current calculation shows that the separated bubble dynamics depends on very complex interactions of large eddies formed in the upstream free shear layer with the wall in the reattachment region and whose corresponding shedding frequency is given by $f.L_r/U_\infty \approx 0.2$. Besides, it has been observed that the secondary corner vortex experiences a cycle of growth and decay. The correspondence between the frequencies of this secondary corner vortex dynamics and the flapping motion ($f.L_r/U_\infty \approx 0.08$) suggests that there should be different aspects of the same motion. Theses results show that there is an ordered structure in this axisymmetric separating/reattaching flow which is dominated by large scale coherent motion. This is confirmed by a two-point correlation analysis of the pressure signals showing that the flow is dominated by highly coherent antisymmetric modes at the flapping and vortex shedding frequencies whose signatures are evidenced in the spectrum of the computed buffet loads. Possible onsets of a large-scale self-sustained motion of the separated area are finally discussed and the existence of an absolute instability of the axisymmetric recirculation bubble originating from a region located near the middle of the recirculating zone is conjectured.

PACS numbers: Valid PACS appear here

I. INTRODUCTION

A. Context

The understanding of the structure of turbulent shear flows with separation and reattachment is of major importance for the design and control of many engineering applications: aerodynamic performance, structural loads or flight control among others. For example, a massive and highly unstable separation occurs in the flow around the afterbody of a space launch vehicle because of an abrupt change in the geometry of the first stage. These recirculating areas are characterized by low pressure levels compared to the freestream conditions, which dramatically increase the base drag. Furthermore, flow separation is a highly three-dimensional process which can result in dynamic loads (also called side-loads) and might disturb the launcher stability. Moreover, these fluctuations can excite a response of the structural modes called buffeting. As a consequence, a better knowledge of the unsteady flow mechanisms involved in the buffet phenomenon[2–5] is necessary for the design of afterbodies of future launch vehicles.

B. Basic physics of afterbody flows

Two-dimensional mean flows featuring separation from sharp edge have been extensively studied in the past numerically and experimentally. Nevertheless, only a limited amount of experimental data on axisymmetrical afterbodies is available and only a few papers are devoted to the unsteady properties of axisymmetrical afterbodies flows. Even on the theoretical side, Roshko[6] stressed the lack of a theory comparable to that of Von Kàrmàn for the two-dimensional vortex street. As an example, Calvert[7] investigated the flow past a cone and observed that the periodic vortex shedding, clearly pronounced in two-dimensional flows[8], does not appear very prominent in an axisymmetric base flow. This fact is also supported by the findings of Gai and Patil[9] who evaluated on a subsonic blunted axisymmetrical base several devices which have proved to yield significant drag reduction in two-dimensional low-speed flows. They observed that these devices do not work as well as in an axisymmetric flow because of the different nature between two and three-dimensional wake flows. Experimental results on more complex axisymmetrical afterbodies have shown that the wall pressure is highly dependent on the geometry (see the review by Délery

and Siriex[10]). More recently, Deprés *et al.*[1] have highlighted the differences featured by several axisymmetric base flow configurations, depending on whether a downstream reattachment of the free shear layer on a solid surface occurs or not. Therefore, two kinds of flow reattachment can be distiguished depending on whether a solid surface is involved in the reattachment process (solid reattachment, category II) or not (fluidic reattachment, category I).

As an example, downstream of a blunt-based body, the flow is characterized by a mutual interaction between the separating shear layers which results in the formation of large scale vortices in the wake. The large scale structures in axisymmetric wakes have been investigated experimentally for different bodies such as spheres, blunted-axisymmetrical base or circular disks. According to the previous classification, this kind of flows belongs to category I and has been mainly studied in low speed flows (see table I). Among them, Taneda[11] showed that a sphere in an uniform flow is subject to a side force at Reynolds numbers ranging from 400 to 10^6 since the sphere wake is not axisymmetric. Berger *et al.*[12] succeeded in identifying three instabilities in the wake behind a sphere characterized by distinct Strouhal numbers ($St_D = fD/U_\infty$ based on the diameter of the sphere and the free stream velocity). The first mode was observed at $St_D \approx 0.05$ and was attributed to an axisymmetric pumping of the recirculating bubble. A highly coherent antisymmetric mode (referred to as mode $m = 1$) at the vortex shedding frequency $St_D \approx 0.135$ defines the second mode. The last mode at $St_D \approx 1.62$ was attributed to an instability of the shear layer. Constantinescu and Squires[13] used Detached Eddy Simulation (DES[14]) to investigate the flow around a sphere for conditions corresponding to subcritical and supercritical regimes. They showed that in the latter one, the wake is characterized by regular shedding of hairpin like vortices. On the experimental side, Higuchi[15] conducted exploratory flow visualization studies and observed both axisymmetric and asymmetric wake structures behind a circular disk. Besides, Fuchs *et al.*[16] investigated the unsteady flow past a circular disk and got interested in the azimuthal structure of the wake by the use of narrow-band two-point space correlation. They showed that the wake is dominated by a vortex shedding possibly organized in a helicoidal structure randomly oriented in the azimuthal direction. As far as axisymmetric blunt base flows are concerned, the most well known feature is probably the static pressure which is found to be nearly constant over the blunt surface (see the review by Délery and Siriex[10]). Unlike

the static pressure behavior, Eldred[17] observed that the rms pressure level is lower at the middle of the base with $Cp_{rms} = 0.007$ and raises as r/R increases to reach $Cp_{rms} = 0.015$ at 65% radius. Deprés *et al.*[1] observed right the opposite behavior since they found that the maximum value of $Cp_{rms} = 0.027$ in the middle of the base and the minimum value $Cp_{rms} = 0.014$ in the outer region.

Of interest a vortex shedding process was shown to exist in the wake at high subsonic regime for high Reynolds numbers. Indeed, Flodrops and Desse[18] investigated the wake of an axisymmetric base flow thanks to hot-wire probes and a Strouhal number $St_D \approx 0.2$ was clearly evidenced in their spectrum of streamwise velocity fluctuations. Nevertheless, the wall pressure spectra do not exhibit any particular contribution at $St_D \approx 0.2$ but are rather centered around $St_D \approx 0.06$. This was also observed by Calvert[7] in the flow past a cone. In addition, Merz *et al.*[19] showed that the maximum backflow velocity U_{max} on the near-wake centerline was $35-40\%$ of the free stream velocity and was found at 60% of the recirculation length L_r. Moreover, the centerline velocity distribution in the recirculation region exhibits a similarity for all approaching subsonic Mach numbers and can be represented by a simple expression derived from a correlation of data which expresses $U/U_{max} = \sin^m [\pi (x/L_r)^n]$ (with $m = 0.612949$ and $n = 1.356915$). It is now established[20] that flows featuring strong reverse flow areas are good candidates to support absolute instabilities. Indeed, to illustrate this it is worthwhile remembering that Monkewitz[21] conducted an incompressible stability analysis of a family of axisymmetric wake profiles showing that the preferred instability mode in the axisymmetric wake is a simple spiral which may be driven by a self-excited oscillation of the wake. Weickgenannt and Monkewitz[22] confirmed the helical vortex structure in the wake of an axisymmetric base flow by using phase-locked measurements of the instantaneous streamwise velocity field. More recently, Sevilla and Martínez-Bazán[23] conducted a linear stability analysis in the wake of an axisymmetric body. They proved the existence of a finite region of absolute instability in the near field of the wake which presumably triggers the large-scale helical vortex shedding. These authors also showed that it was possible to inhibate the vortex shedding of an axisymmetric body by blowing a certain mass flow through the blunted base. It is well known since the early 1960s that the von Kármán vortex street can be suppressed by using base bleed[24,25], splitter plates[26], suction, or other geometrical manipulations. Such devices allow to avoid the absolutely unstable wake region behind two-dimensional blunt bodies through the modification of the mean velocity profile

in the separated region.

The second kind of base flow separations (i.e. of category II) occurs when the free shear layer interacts with a solid wall through the reattachment process. There has been a huge amount of quite detailed studies of separated turbulent (mainly low-speed) flows behind backward facing steps (see the reviews by Eaton and Johnston[27], Bradshaw and Wong[28]), fences and flat plate leading edges (see table II). Two basic modes of characteristic frequencies are found in all the abovementioned flow configurations. The lower frequency mode reflects an overall growth/decay dynamics of the entire bubble or shear-layer "flapping" as it is often called in the litterature. The higher frequency mode is the Kelvin Helmholtz instability of the free shear layer. A second kind of vortical motion is also observed and attributed to a vortex-shedding instability. The review by Mabey[29] on wall pressure fluctuations in recirculating regions covering a wide-range of separating-reattaching flows has shown that a good scaling parameter is the size of the mean separated bubble L_r. Indeed, the dominant flow unsteadiness is characterized by a Strouhal number $fL_r/U_\infty \approx 0.6$. Based on an analogy with cylinder vortex shedding, Sigurdson[30] proposed an other frequency scaling based on the bubble height h and the velocity at the separation point denoted by Us. He showed that non-dimensionalized shedding frequency $fh/Us \approx 0.08$ correlates well with unsteady data taken from a wide range of configurations where the flow reattaches on walls. He stressed that this result may appear quite surprising because separating bubbles reattaching on walls have symmetry imposed by the reflection condition while Kármán vortex shedding is unsymmetrical.

However, less attention was paid to the analysis of the spatial organization of the fluctuating pressure field in case of an axisymmetric separating/reattaching flow than to its two-dimensional counterpart. One of the objectives of this study is to provide further insight into the unsteady nature of an axisymmetric separating-reattaching flow.

C. Organization of the paper

The paper is organized as follows. In Sec. II we briefly present the numerical methods and the modelling used. The characteristics of the test case are presented in Sec. III which includes the description of the computational grids. The Reynolds-averaged data including

the mixing layer properties and the wall pressure are compared with the available experimental data and with those of classical backward-facing step flows in Sec. IV. The spatial organization of the fluctuating pressure field is presented in Sec. V which includes spectral and two-point analysis as well as the description of the resulting buffet loads. Finally, some details of the self-sustained oscillation mechanism of this afterbody step-flow are discussed in Sec.VI with the help of instantaneous visualizations and of a propagating disturbance analysis.

II. NUMERICAL METHOD

A. General description

The solver FLU3M code developed by ONERA solves the compressible Navier-Stokes equations on multiblock structured grids. The time integration is carried out by means of the second-order-accurate backward scheme of Gear. In the present study, the Euler fluxes are discretized by using a Roe scheme (third-order upwind biased). Further details concerning the numerical method and implementation of turbulence models can be found in references[31,32].

The accuracy of the solver for DNS, LES and hybrid RANS/LES purposes has been assessed in various applications including transitional flows around a two-dimensional wing profile in near-stall conditions[33], cavity flows at high Reynolds number[34], synthetic jets in a cross flow[35] and afterbody flows[4].

B. Zonal Detached Eddy Simulation

Because of the high Reynolds number of the flow under consideration, the approach used in the present work is the Zonal Detached Eddy Simulation (ZDES)[36] which is derived from the classical Detached Eddy Simulation introduced by Spalart *et al.*[14]. The two approaches mainly differ by the fact that within ZDES, the user has to select individual RANS and LES domains while standard DES is a non-zonal approach. One of the objectives of ZDES is to shield attached boundary layers from any modelled-stress-depletion issue (see the recent discussion by Spalart *et al.*[37]) especially in presence of thick incoming boundary layers. This approach is well-adapted when detachment occurs near the sharp edges of the body with

associated large variations in velocity and pressure downstream. In all cases, these methodologies are part of the RANS/LES family (for more details, see the review by Sagaut, Deck and Terracol[38]).

The ZDES approach has been successfully used to predict the transonic buffet phenomenon over a supercritical airfoil[39], the flow around a high-lift configuration[36] as well as to investigate supersonic base flow aerodynamics under highly compressible conditions[40].

III. TEST CASE

A. ONERA experiment

The afterbody retained for this numerical study was originally designed to be representative of a space launcher vehicle first stage. Nevertheless, some features detailed below make this flow particularly well suited to investigate axisymmetric separating/reattaching flows at high Reynolds number. The experimental study on axisymmetric base flows has been carried out in the S3Ch continuous research wind tunnel of ONERA's Chalais Meudon center. The test section is square shaped, and the dimensions of the test chamber are $0.78 \times 0.78\, m^2$. A detailed description of the experimental set-up, equipment, and results is given by Deprés[41] and Deprés *et al.*[1].

The general configuration is an axisymmetric body of diameter $D = 100\, mm$ prolongated by an emergence of lower diameter and of finite downstream extension L such as $L/D = 1.2$ (see figure 1). It is immersed into a high subsonic flow with a free stream Mach number of 0.702 leading to a Reynolds number based on the forebody diameter D of about $Re_D \approx 1.1\, 10^6$. Besides, an ideal truncated contoured nozzle (TIC) is integrated in the extension base center leading to an adapted supersonic jet characterized by a nozzle pressure ratio $NPR \approx 34$. In addition, the initial external boundary layer thickness δ was measured using a pitot rake at $X/D = -2.45$ and the ratio δ/D was found to be equal to 0.2. The model was equipped with both steady pressure taps and unsteady Kulite sensors to record simultaneously the fluctuating wall pressures.

B. Grids and description of the computation

The grid generation constitutes an important issue because the grid extension controls which wavelengths can be resolved as well as the eddy viscosity level. A well-choosen grid topology allows one to minimize the number of total grid points while achieving the proper mesh distribution and maintaining the desired level of accuracy in the region of interest. Therefore, the structured multiblock mesh is made up of 25 blocks and is based on an O-H topology to avoid singularity problem near the axis. A cut-away view through the mesh around the afterbody is displayed in figure 2. It is noteworthy that a special care has been taken to achieve a good cell isotropy in the LES region (i.e. separated area). To assess the effect of grid distribution on the averaged data, three grids have been built whose main characteristics are gathered in table III. Grids M1 and M2 differ by the number of points in a plane of symmetry while having the same azimuthal resolution. Grid M3 differs from grid M1 by a higher azimuthal discretization.

As reminded in Sec II, within ZDES, the user has to select individual RANS and LES domains. The nozzle flow as well as the attached boundary layer on the main cylinder (i.e. for $X \leq 0$) are explicitly treated in RANS mode to avoid any modelled stressed depletion while the LES mode of DES is retained for $X > 0$. After the transient phase, the real unsteady calculation begins allowing to collect statistics. The computation and post-processing of the results are based on nondimensionalized flow quantities. The average procedure is performed in time during the calculation. The CPU cost per cell and per inner iteration is less than $10^{-6}s$. The simulations are performed on a single processor of a NEC-SX6 supercomputer and the code is running approximatively at 4×10^9 floating-point operations per second. The time step is fixed to $\Delta t_{CFD} = 2\mu s$ which corresponds to a non-dimensionnalized time-step $\Delta\tilde{t} = \Delta t_{CFD} U_\infty / H = 1.58\,10^{-2}$ with 4 Newton inner iterations yielding a maximum Courant-Friedrich-Levy number based on acoustic velocity ($U+a$) equal to 40 (located at the separation edge). Temporal accuracy of the calculation was checked during the convergence process of the inner-iterations (a drop of the residuals of at least one order is reached). The useful unsteady calculation is performed over a total duration of $T.U_\infty/H = 1500$.

IV. RESULTS AND DISCUSSION

A. Instantaneous and time-averaged flowfields

The main characteristics of the instantaneous flowfield are presented in Figure 3. The turbulent structures are evidenced by showing a positive iso-value of the $\mathcal{Q}$-criterion[42]. It defines as vortex tubes the regions where the second invariant of velocity gradient tensor $\mathcal{Q}$ is positive :

$$\mathcal{Q} = \frac{1}{2}\left(\Omega_{ij}\Omega_{ij} - S_{ij}S_{ij}\right) = -\frac{1}{2}\frac{\partial u_i}{\partial x_j}\frac{\partial u_j}{\partial x_i} > 0 \tag{1}$$

where S_{ij} and Ω_{ij} are respectively the symmetric and antisymmetric components of ∇u. One can notice at first the roll-up of azimuthal vortical structures which grow by pairing and are rapidly replaced by large three-dimensional structures developing as the shear layer approaches reattachment. Note also the occurrence of large scale hairpin vortices in the reattachment zone.

This time dependent aerodynamic field is then time averaged during the calculation. The streamwise velocity magnitude, streamlines and pressure coefficient contours are displayed in figure 4. One can distinguish the recompression shock in the supersonic jet exhausting from the nozzle as well as the base flow. The external flow expands at the base corner and is followed by a recompression downstream of the base, which realigns the flow. A low-pressure region is formed immediately downstream of the edge, characterized by a low-speed recirculating flow region. A secondary vortex is also evidenced in the corner. Interaction between this recirculating region and the external flow occurs through the free shear mixing region. This averaged flowfield also shows strong backflow near the middle of the recirculation zone, which reaches more than 30% of the free stream velocity at $X/L_r \approx 0.6$ (see again the results obtained by Merz *et al.*[19] in the case of an axisymmetric base flow). According to Mabey[29], the mean reattachment length is an important scaling parameter for the present flow study. It was found to be $L_r/D \approx 1.1$ which is in accordance with the measurements of Lê *et al.* and Coe (see table II). In their paper, Dépres *et al.*[1] indicate that in the case of an axisymmetric rearward facing step, the reattachment length was $L_r/D \approx 1.3$ using oil flow visualization. Moreover, they showed that the presence of the jet had no influence on the rear-body pressure distribution due to the reattachment of the shear layer on the body

which isolates the recirculating area from the jet.

B. Mixing layer mean flow analysis

Similarly to backward facing step flows, the free shear layer plays an important role in the global dynamics of the axisymmetric bubble since the interaction of large eddy structures (figure 3) with the wall in the reattachment region are formed in the upstream free shear layer. Thus, this section focuses on some important properties of the separating mixing layer and compare them with those encountered in other classical shear flows.

Therefore it is worth analyzing the streamwise evolution of the characteristic thicknesses of the shear layer. Among them, the vorticity thickness is given by:

$$\delta_\omega(x) = \max_y \left[\frac{U_\infty - u_{min}}{\frac{\partial < u > (x,y)}{\partial y}} \right] \tag{2}$$

where U_∞ denotes the free-stream velocity, $< u > (x,y)$ is the time-averaged streamwise velocity and $u_{min} = \min_{[y]}(< u > (x,y))$. One can also define the momentum thickness $\theta(x,y)$:

$$\theta(x) = \int_{y_{min}}^{+\infty} \frac{< u > (x,y) - u_{min}(x)}{U_\infty - u_{min}(x)} \left(1 - \frac{< u > (x,y) - u_{min}(x)}{U_\infty - u_{min}(x)} \right) dy \tag{3}$$

The streamwise evolution of the vorticity thickness is displayed in figure 5 which evidences three regions. The first one is located between $X/L_r = 0$ and $X/L_r = 0.2$ where the growth of the mixing layer is exponential as predicted by linear stability theory in the case of planar mixing layers. At this stage, it is also worthwhile to remember the work by Husain and Hussain[43] who studied experimentally an axisymmetric mixing layer. They observed that relevant parameters including spread rate, vorticity thickness and streamwise velocity fluctuations were in both qualitative and quantitative agreement with planar mixing layer results. The second region evidenced in figure 5 is wider and characterized by a nearly linear rate $d\delta_\omega/dx = 0.36$. This value is twice as high as those observed in classical planar mixing layer since Ho and Huang[44] found a growth rate equal to $d\delta_\omega/dx = 0.17$ (assuming a velocity ratio $\frac{U_\infty - u_{min}(x)}{U_\infty + u_{min}(x)} = 1$). In our case, the low-speed side flow of the mixing layer is highly turbulent due to the recirculation. Indeed, turbulent structures are reingested in the mixing layer thus enhancing its growth. In the last region, i.e. for $X/L_r \geq 0.5$, the mixing

layer is strongly affected by the reattachment process and the vorticity thickness reaches a plateau. This result is in accordance with the observations of Cherry et al.[45] who found that up to 60% of the separation length the mixing layer grows in relative isolation from the effects of the rettachment process.

Figure 5 also displays the ratio between the momentum and vorticity thicknesses. The peak observed near $X/L_r \approx 0.15$ is due to the corner flow and more precisely to the definition of u_{min} appearing in eq. 3. Note that δ_ω/θ lies in the range 4-5 for $X/L_r \geq 0.5$. Castro and Haque[46] got interested in the properties of a mixing layer developing downstream of a normal plate and observed that the ratio between the vorticity and momentum thicknesses was close to 5. A similar value has been reported by Dandois *et al.*[47] in the case of a rounded ramp ($\delta_\omega/\theta \approx 4.7$) and by Larchevêque *et al.*[48] ($\delta_\omega/\theta \approx 5$) who investigated cavity flows.

In addition, the peak of Reynolds stresses in the mixing layer can be compared with those encountered in classical shear flows including planar and axisymmetric mixing layers as well as fence and backward facing step flows (see table IV). The maximum level of $u_{rms}/\Delta u$ is close to those observed in two-dimensional backward facing step flows. However, the maximum level of $v_{rms}/\Delta u$ is higher than in the experiments of Jovic[49] and Chandrsuda and Bradshaw[50] but lower than in the experiment of Castro and Haque[46]. These latter authors observed that normal stresses are always higher than in a planar mixing layer and concluded that the re-entrainment of the recirculating fluid back into the shear layer is the dominant mechanism explaining the maintenance of the high normal stresses. The differences between the geometries and the associated amount of backflow reingested in the mixing layer can thus partly explain the discrepancies observed in the peak normal stresses. Moreover, the maximum value of the shear stress $\sqrt{-u'v'}/\Delta u$ is close to the value found by Castro and Haque[46].

Finally, this axisymmetric step flow shares many similar features with the two-dimensional backward facing step flows as regards the shear-layer instability process.

C. Mean and fluctuating pressure distribution

This section focuses on the wall pressure statistical properties along the emerging body.

To begin, figure 6 compares the computed streamwise evolution of the pressure coefficient $Cp = \frac{P-P_\infty}{q_\infty}$ ($q_\infty = \frac{1}{2}\rho_\infty U_\infty^2$) with the experiment. Three different regions can be

distinguished.

On the main cylinder (i.e. $X/L_r \leq 0$), one can notice a slow decrease of Cp as the streamwise location increases which highlights the upstream influence of the recirculation region on the attached boundary layer. Indeed, the local flow adjacent to the body accelerates as the blunt base is approached. Merz *et al.*[19] investigated the turbulent near wake of a cylindrical blunt based body and observed that the influence of the near wake extends at least three body diameters upstream of the separation point. The second region shows a small decrease of Cp in the separation region from $X/L_r = 0$ up to $X/L_r = 0.5$ due to the acceleration of the backflow. Note that the averaged Cp value in this region ($Cp = -0.17$) is slightly higher than in the blunt base flow case ($Cp = -0.14$) in similar free stream conditions (see table I). The last region is characterized by a strong recompression process where the amplitude Cp_{max} is reached downstream of the mean reattachment point (at $X/L_r \approx 1.1$) which corroborates with earlier findings in two-dimensional backward-facing step flows[51,52].
Note that this pressure distribution is well reproduced by ZDES and that only small differences are observed between the different grids.

The root-mean-square (rms) coefficient of the pressure fluctuation $Cp_{rms} = \overline{P'^2}/\frac{1}{2}\rho_\infty U_\infty^2$ (where $P^{'}$ is the fluctuating pressure) is shown in figure 7.

It increases steadily in the streamwise direction downstream of the base and reaches a plateau just upstream of the mean shear layer reattachment location ($Cp_{rms} \approx 0.05$) at $X/L_r = 0.8$. Lê[53] studied a similar configuration ($L/D = 1.22$ and $M_\infty = 0.8$) and found higher value of $Cp_{rms} = 0.07$. Mabey[29] noted that this maximum seems relatively insensitive to wide changes in Reynolds numbers. It is also worth noting that the rms value begins to increase rapidly at about $X/L_r \approx 0.5$, which is the location where the pressure coefficient Cp also begins to rise (see figure 6). Hudy *et al.*[54] reminded that this increase in rms is likely due to the organized shear layer structures which get stronger and move closer to the wall. Furthermore, the rms value decreases only slowly after reattachment. In the case of two-dimensional backward facing step flows, Lee and Sung[52] suggest that this implies that a large-scale vortical motion persists after reattachment as we will be discussed in the following. This characteristic behavior of the fluctuating pressure in the recirculation region when solid reattachment occurs has been fully described by Mabey[29] and is observed

for many bubble type separations. For example, Coe[55] measured behind a step on a body of revolution at $M_\infty = 0.8$ that the maximum fluctuating pressure level reached a value $Cp_{rms} = 0.06$ and was located at $X/L_r \approx 0.73$. Similar levels where also reported by Kumar *et al.*[56] ($Cp_{rms} = 0.05$) in the case of an axisymmetric step and Mabey[57] ($Cp_{rms} = 0.06$) in the case of a backward facing-step at $M_\infty = 0.33$ (see tab II).

The experimental values have been obtained by integrating the pressure spectra for normalized frequencies lower than $St_D \leq 2$. Hence, the computed statistical rms values (i.e. defined over the all frequency range) are compared to the experimental values and to the numerical values computed in the same way as in the experiment (i.e. integrated for $St_D \in [0.02; 2]$). One can notice that only minor differences between the two frequency ranges are observed showing that frequencies higher than $St_D = 2$ are negligible contributors to the energy of pressure fluctuations.

Figure 7 also highlights the importance of grid refinement on the computed fluctuating level. Indeed, calculations on grids M1 and M2 overestimate by nearly 40% the rms level at reattachment though minor differences were observed on the mean field. Let us recall that these grids differ by the number of points in a plane of symmetry while having the same azimuthal discretisation ($N_z = 97$). A significant improvement is obtained with M3 grid which differs with grid M1 by a higher azimuthal resolution ($N_z = 144$). Figure 3 has shown the roll-up of toroïdal eddies which are then destabilized by azimuthal instability modes. This process may be altered by an insufficient azimuthal discretisation leading to over-coherent structures resulting in too high fluctuating levels. This result reveals the importance of the azimuthal discretisation when assessing fluctuating pressure levels in an axisymmetric configuration since unsteadiness is mainly imposed by the annular shear layer.

V. SPATIAL ORGANIZATION OF THE FLUCTUATING PRESSURE FIELD

A. Spectral analysis

The Power Spectral Density (PSD) function of pressure fluctuations, named $G(f)$ and expressed in Pa^2/Hz describes how the mean squared-value of the wall pressure previously described is distributed in frequency[58] since:

$$\sigma^2 = \int_0^\infty G(f)df = \int_0^\infty f.G(f)d\left[\log\left(f\right)\right] \tag{4}$$

Therefore, by plotting spectra as $f.G(f)/\sigma^2$ in linear/log axis, one can obtain directly the contribution to the total energy of the considered frequency band.

Figure 8 compares the spectra of wall pressure fluctuations for several stations along the model to the experimental data. One can notice that the pressure spectra display different frequency contributions depending on their position in the recirculation bubble. Indeed, close to separation (at $X/L_r = 0.148$) where the amplitude of pressure fluctuation is weak (see figure 7), the spectrum is dominated by a low frequency contribution since roughly 65% of the energy is contained at $fL_r/U_\infty \leq 0.12$. This spectrum also displays a peak at $fL_r/U_\infty \approx 0.08$ close to what is observed in two-dimensional separating/reattaching flows (see table II). This low frequency peak is often attributed[51] to the "flapping" of the shear layer and reflects the overall separation-bubble growth/decay dynamics. Cherry *et al.*[45] noted that this low frequency scales best upon the reattachment length and identified the motion as one related to the overall bubble scale. This point will be disccused in further details in Sec. VI.

Moving farther downstream the spectra become dominated by a broadband high frequency contribution since these organized shear layer structures which grow in strength move closer to the wall before crashing against it and breaking into smaller scales. Note also that this broadband contribution is centered around $fL_r/U_\infty \approx 0.6$ which agrees with Mabey's[57] earlier findings. This is the characteristic frequency of vortical structures seen in free shear layers since $St_{L_r} \approx 0.6$ corresponds to $St_{\delta_\omega} \approx 0.132$ (with $\delta_\omega/D \approx 0.22$ and $L_r/D \approx 1.1$ see figure 5). This value agrees well with the estimation of the local most amplified frequency of a linear stability analysis in case of a two-dimensional mixing layer as estimated by Huerre and Rossi[59]: $f_{KH}(x) \approx 0.135.\overline{U}/\delta_\omega(x)$. In addition to this broadband contribution, there is a weakly defined local maxima at $fL_r/U_\infty \approx 0.22$ (or $fD/U_\infty \approx 0.2$) especially near the middle of the recirculating area that will be discussed in the following.

Besides, the wall pressure spectra reflect the footprint of the propagating disturbances in the aerodynamic field. To strengthen the interpretation of the different frequency contribution in the pressure spectra, it is worth analyzing the spectral content of the velocity field in a few stations of interest. Thus, figure 9 displays the spectrum of the vertical velocity component for two points located in the shear layer. The first one is

located 1.6 step heights downstream of the base and exhibits a peak at $fL_r/U_\infty \approx 0.06$ characterizing the flapping of the shear layer, i.e. its vertical motion. This spectrum also displays a broadband content at much higher frequencies which corresponds to the signature of the shear layer instability process. The second point is still located in the shear layer but is already affected by the reattachment region. The velocity spectrum for this sensor clearly exhibits a peak near $fD/U_\infty \approx 0.2$ which can be attributed to a vortex shedding phenomenon of the entire bubble as will be seen in Sec. VI.

The previous spectra have shown for several streamwise locations on the body, how the energy is distributed in the frequency domain. Concurrently, it is now worthwhile to assess which length scale contributes preponderantly to the low-frequency fluctuations of the pressure field. Therefore, let us for instance consider the instantaneous aerodynamic field in a section located normally to the inflow at an arbitrary time instant t_0 in the second-half of the recirculation zone at $X/L_r = 0.67$ as shown in figure 10. One can firstly notice the mushroom-shape structures in the mixing layer reflecting the existence of streamwise vortices (see the hairpin vortices in figure 3) as well as smaller scales in the backflow region. Let us now consider the instantaneous azimuthal pressure distribution for three crowns of sensors located respectively in the shear layer, in the middle of the recirculation zone and near the wall. For each crown, one can compute the spectra of pressure fluctuations in the azimuthal wave number $G_{P'}(k_\theta, t_0)$ space as a function of the non-dimensionalized azimuthal wave number $k_\theta.P$ where $P = 2\pi r$ denotes the perimeter of the crown located at the radial position r. The occurrence of the several peaks in the mixing layer (see figure 10) reflects the contribution of the structures characterized by their azimuthal wave number to the energy of the instantaneous pressure field. These instantaneous spectra $G_{P'}(k_\theta, t)$ can then be averaged in time to evidence which azimuthal length scale is, in a statistical sense, mainly excited. It is noteworthy in the previous figure that these time-averaged spectra display a peak at $k_\theta P \approx 2$ or in other words that the most contributing spatial length in the azimuthal direction to the energy of pressure fluctuations involves two-points diametrically opposite. This result is of primary importance due to its relevance to side-loads as discussed in the following.

B. Two-point analysis

The spectral analysis has highlighted different frequency contributions depending on the location in the separated area as well as the azimuthal length scale contributions to the energy of pressure fluctuations. To get further insight into the spatial organization of the flow at these frequencies, one can consider the azimuthal coherence of two pressure sensors $p_1(r, X, \phi_1)$ and $p_2(r, X, \phi_2)$ located in a plane normal to the inflow $X \equiv constant$ and at constant radius $r \equiv constant$. Assuming the hypothesis of an homogeneous flow, i.e. there should not be any preferred angle of reference ϕ_1, the complex coherence function may be expressed as:

$$\begin{aligned} C(f, r, X, \Delta\phi) &= (C_r + jC_i)(f, r, X, \Delta\phi) \\ &= \frac{S_{12}(f, r, \Delta\phi, X)}{\sqrt{S_1(f, r, \phi_1, X)\, S_2(f, r, \phi_2, X)}} \end{aligned} \tag{5}$$

where C_r and C_i are respectively the real and imaginary part of the cross-spectral density function S_{12} and $\Delta\phi = \phi_1 - \phi_2$. Assuming now that the disturbances do not exhibit any particular direction of propagation $S_{12}(\Delta\phi) = S_{12}(-\Delta\phi)$, the hypothesis of isotropy yields $C_i = 0$. The C_r function is 2π periodic with respect to $\Delta\phi$ and can be expressed thanks to a Fourier transform in azimuthal modes:

$$C_r(f, \Delta\phi) = \sum_{m=0}^{\infty} C_{r,m}(f) \cos(m\Delta\phi) \tag{6}$$

$C_{r,m}$ represents the percentage of the fluctuating energy at frequency f relative to the azimuthal mode m since $\sum_m C_{r,m} = 1$. In addition, the analysis of the non-symmetric mode is of primary interest with view to the side-loads[60] problem. Note also that no conditional sampling of the natural occurring fluctuations is required. This analyzing technique has been used by Fuchs *et al.*[16] in the case of a flow past a circular disk and has been revisited recently by Deprés *et al.*[1].

Figure 11 shows the $C_{r,m}$ spectrum for the axisymmetric mode ($m = 0$) and the anti-symmetric mode ($m = 1$) for three different locations in the separated area. Let us remind that the $m = 0$ mode is characterized by an inphase relationship of signals recorded simultaneously by probes facing each other. An anti-phase relationship characterises the $m = 1$ mode.

The $m = 0$ contribution is confined at low frequencies and decreases continuously with increasing frequencies which is not inconsistent with a small-scale homogeneous and

isotropic turbulence field. Of great interest is the spectrum of $C_{r,1}$ at $X/L_r = 0.67$ which displays a peak near $fD/U_\infty \approx 0.2$ and shows that experimentally more than 50% of the pressure fluctuations at this frequency are due to this anti-symmetric mode. According to Fuchs *et al.*[16], the mode $m = 1$ can be related to helical vortex structures randomly oriented in the azimuthal direction. Although the time-averaged flow is axisymmetric, the occurrence of this anti-symmetric mode seems to be a robust feature of axisymmetric flows. Indeed, Deprés[41] investigated experimentally the effect of the rear body extension and the presence of a jet in the organization of the wall pressure field. He showed the existence of the $m = 1$ mode whether the separated shear layer interacts with a solid wall (solid reattachment, present case), a supersonic jet or not (fluid reattachment). In this latter case, i.e. when the flow is characterized by a mutual interaction between the separating shear layers, Deprés *et al.*[1] reported that the antisymmetric mode can contribute more than 90% to the pressure fluctuations at the vortex shedding frequency. Both experimental[1] and numerical studies[61] showed that this particular azimuthal correlation of the wall pressure fluctuations still exist when the external flow interacts with a supersonic jet. Nevertheless the mode $m = 1$ is then more weakly defined as in the case of a fluidic reattachment process(category I) without jet. As noted by Deprés[41], this result suggests a somewhat less organised flow. This is partly due to the small scale turbulence generated by the interaction of the free shear layer with a solid wall or with a supersonic jet (more or less acting as a solid wall).

C. Buffet Loads

In all cases, the occurrence of highly coherent antisymmetric fluctuations on the body surface induces unsteady asymmetrical loads. These loads can be obtained by integrating the unsteady pressure field on the rear body surface during the calculation. Figure 12 shows a typical polar plot of the side-loads (i.e. $Fy(t)$ component of the load versus $Fz(t)$), together with its $\alpha = 0.95$ confidence ellipse which includes 95% of the observations and whose boundary in $\mathcal{R}^2$ space is defined by:

$$\left(\tilde{F} - M\right)^t C^{-1} \left(\tilde{F} - M\right) = 2 \log\left(1 - \alpha\right) \tag{7}$$

where $\tilde{F} = (Fy, Fz)^t$ denotes the bidimensional random variable defined by its mean value $M = \left[\overline{Fy}\,\overline{Fz}\right]^t$ and its covariance matrix $C = \overline{\tilde{F}\tilde{F}^t} - MM^t$. One can notice the isotropic (i.e. $\sigma_{Fy} = \sigma_{Fz}$ and the ellipse becomes a circle) and random character of the fluctuating side-load. The envelope of the loads is centered at zero since for an averaged axisymmetric flow the buffet load is absent, that is $\overline{Fy} = \overline{Fz} = 0$. One can show (see the discussion by Deck and Nguyen[60]) that this buffet load can be seen as a rotating vector uniformly distributed within the interval $[0, 2\pi]$ (i.e. no direction is privileged) and whose magnitude $\sqrt{F_y^2(t) + F_z^2(t)}$ follows Rayleigh's law (particular case of a χ^2 distribution with two degrees of freedom). This last result simply means that the side-loads components are normally distributed. Figure 13 presents the PSD of the $F_y(t)$ component of the buffet load. More than 80% of the energy of buffet loads are observed for normalized frequencies $f.L_r/U_\infty \leq 0.5$ and especially in the frequency band $f.L_r/U_\infty \in [0.15; 0.25]$ which contributes to 30% of this side-load. A broad band contribution centered near $f.L_r/U_\infty \approx 0.08 - 0.1$ is also evidenced. These results are consistant with the two-point analysis which highlighted that the pressure field on the rear body is anticorrelated at frequencies $f.L_r/U_\infty \approx 0.08$ and 0.2 (see figure 11). The higher frequency peaks are narrow and contribute weakly to the buffet load.

VI. FURTHER DISCUSSION ON SELF-SUSTAINED OSCILLATION

The first part of this study has revealed the occurrence of large scale coherent motions resulting in self-sustained pressure oscillations. Many scenarii have been advanced by several authors to explain the occurrence of self-sustained motions but only a few of them have been supported with flow visualizations especially in the case of axisymmetric flows. Among them, Cherry *et al.*[45] investigated the dynamics of the separated bubble downstream a blunt-face splitter plate. Thanks to instantaneous smoke visualizations, these authors observed shedding of pseudo periodic trains of vortical structures. In the case of a turbulent reattachment behind a backward facing step, Driver *et al.*[51] observed an important contraction and elongation of the separated bubble due to the shortening and lengthening of the reattachment length. It is also worthwhile to remind the work by Pronchick and Kline[62] who proposed a qualitative model of the reattachment process. Based on visualization in a low-velocity water channel, these authors distinguished two groups of structures in the reattachment region: "overriding" and "interacting" eddies. The overriding eddies pass over

the reattachment zone without being largely altered while the impinging eddies that strike the wall lose their large-scale coherence.

In our axisymmetric case, the motion of the separated area is illustrated in figure 14 which presents a sequence of selected numerical schlieren snapshots. It appears clearly that the separated bubble dynamics depends on very complex interactions of large eddies formed in the upstream free shear layer with the wall in the reattachment region. One can firstly notice the growth of the shear layer through the pairing process. The impingement zone is then characterized by very large-scale, unsteady and three-dimensional eddies which exhibit wide variations in scale and in trajectories. Conversely, no large-scale turbulent structures are observed in the backflow. One may also notice the formation of very large eddies which agglomerate (see instant $t_0 + 1.32ms$) before being advected and which have a size are comparable to the step height in the present case. It is also observed that the instantaneous reattachment location moves over a distance up to 30% of the mean reattachment length (or one step height) which is in accordance with the observations concerning two-dimensional backward facing step flows. In his review, Simpson[63] reminded that in this latter step flow configuration, the short-time-averaged reattachment location deviates from the long-time-averaged reattachment location by as much as ± 2 step heights.

From figure 14, one now get an estimate of the frequency of this large scale motion at 450Hz (i.e. $St_{L_r} \approx 0.2$) which corroborates the peak observed in the spectrum in the reattachment region at location $X/L_r = 0.670$.

It is also worth getting interested in the dynamics of the corner secondary vortex which has so far received very little attention in the literature[64] especially in axisymmetric step-flows. In order to provide further insight into the behavior of the vortical flow in the near-step region with reference to the low frequency unsteadiness, figure 15 displays the instantaneous pseudo-streamlines and highlights the streamwise ($u > 0$) and reverse ($u < 0$) flow areas. It is evidenced that the corner region is highly unsteady since at time t_0 the size of the secondary vortex becomes of the order of magnitude of the step height. At $t_0 + 2.72ms$, the secondary vortex has almost disappeared while at time $t_0 + 5.4ms$, both primary and secondary vortex can be seen again, the size of the latter being comparable to the step height. This secondary vortex dynamics influences the shear layer motion and one can conjecture from figure 15, the existence of a cycling behavior (i.e. self-sustained motion) whose frequency may be estimated by $f \approx 185\,Hz$ (i.e. $St_{L_r} \approx 0.08$). This frequency

corroborates the peak observed in the spectrum close to the step at location $X/L_r = 0.148$ (see figure 8). These results are in qualitative agreement with the findings of Spazzini *et al.*[65] in case of a two-dimensional backward facing step flow. Through flow visualizations, these authors observed that the secondary corner vortex goes through a process of growing until its size almost reaches the step height and then breaks down. The frequency of this quasi-periodic motion was comparable to the flapping frequency (see table II). They concluded that the correspondence between the frequencies of the flapping motion and the secondary corner vortex dynamics suggests that there are different aspects of the same motion. However, it is difficult to say which phenomenon really triggers the overall motion.

Self-sustained pressure oscillations have been observed for a wide range of spatially developing shear flows. Chomaz *et al.*[66] remind that the origin of these self-sustained motions can be either due to a hydro-acoustic resonance or driven by purely hydrodynamic means. The first class of flows classically involves a spatially developing shear layer impinging a solid surface located farther downstream which gives rise to monochromatic acoustic radiations due to a feedback process. Cavity flows[67], transonic buffet[68,69] causing large-scale self-sustained motion of a shock over the upper-side of an airfoil, etc belong to this kind of flow regimes. The second class of self-sustained oscillations does not need any downstream body and may appear when the flowfield exhibits a region of local absolute instability (see the paper by Huerre and Monkewitz[70] for a detailed description of the local and global instability concepts). These classes of onset of self-sustained motions will be discussed respectively in the two next sections.

A. Possibility of an hydro-acoustic feedback loop

The snapshots shown in figure 14 have already highlighted the occurrence of pressure waves leading to possible feedback process. In this section, we briefly investigate such a possibility.

A wide range of massively separated flows are characterized by shear layers exhibiting self-sustained pressure oscillations. In most cases, this self-oscillating mixing layer impinges upon a solid surface and a model based on acoustic resonance proposed by Tam[71] (see also

discussions in the papers by Rockwell[72], Rockwell and Naudasher[73] and Ho and Nosseir[74]) is often used to get the characteristic frequency of the oscillation:

$$\frac{\mathcal{L}}{u_d} + \frac{\mathcal{L}}{a} = \frac{n}{f} \tag{8}$$

where $\mathcal{L}$ represents the length over which the shear layer develops, a the speed of the sound associated to the upstream travelling disturbance, u_d the speed of the downstream travelling wave and $n = 1, 2, ..$ the stage of the oscillation (vortex pairing, wake oscillation, ...).

As an example Kiya *et al.*[75] used this model to study the unsteadiness of the separated bubble in the case of a blunt-faced splitter plate. These authors argued that when a vortex impinges on the body surface in the reattachment region, an upstream travelling wave at the sound velocity is generated. The pressure fluctuation is received by the flow at the sharp separation edge, which modifies the roll-up instability process in the shear layer. More precisely, the downstream perturbation with an average velocity u_d arrives at the separation point L_r at time L_r/u_d. In their low-speed experiment $u_d << a$ and assuming $n = 1$, eq. 8 reduces to:

$$f_{shedding} L_r / U_\infty \approx 0.5 \tag{9}$$

Since this value is observed in a wide range of separation bubbles, Kiya *et al.*[75] suggested that this feedback mechanism is universal.

In our high-speed axisymmetric configuration, the hypothesis $u_d << a$ does not hold any more. Nevertheless, $\mathcal{L}$ can be taken as the reattachment length $L_r \approx L$ and u_d as the advection velocity of structures in the shear layer $u_d \approx \chi U_\infty$, the use of eq. (8) yields:

$$St_{L_r} = \frac{f L_r}{U_\infty} = n. \frac{\chi}{1 + \chi M_\infty} \tag{10}$$

Assuming $\chi = 0.6$ (which will be determined in the next section) and $M_\infty = 0.702$, yields $St_{L_r} = 0.42$ for $n = 1$ and 0.84 for $n = 2$ which does not evidence the low frequency contribution near the base. In other words, the low frequency motions at $St_{L_r} = \mathcal{O}(0.08)$ and $St_{L_r} = \mathcal{O}(0.2)$ cannot be linked straightforwardly to an aero-acoustic feedback.

The occurrence of pressure waves in the outer field being advected upstream (see figure 14) is due to the impact of large structures being convected after reattachment on the wall

with the supersonic jet acting as a fluidic wall. Let us remind that Deprés *et al.*[1] showed that the presence of the jet had no influence on the rear-body pressure distribution (including spectral distribution) due to the reattachment of the shear layer on the body which isolates the recirculating flow from the jet. The mechanism suggested by Kiya et al. relates to the feedback of disturbances from the separation point to the reattachment. However, the next section will show that the strongest feedback disturbances do not originate from the reattachment point.

B. Analysis of propagating disturbances

The previous discussion (Sec V) has shown that an orderly structure exists in the present axisymmetric separating/reattaching flow. It is dominated by a large-scale coherent motion associated with anti-symmetric pressure fluctuations. The characteristic frequencies of this self-sustained motion do not seem to be directly related to an hydro-acoustic feedback. In order to get more insight into the origin of this self-sustained motion, the propagating wave components of the wall pressure signature are investigated in this section.

Before proceeding further, it is worthwhile to look at the space-time characteristics of wall-pressure fluctuations. Therefore, figure 16 exhibits the space-time contours of the instantaneous wall-pressure fluctuations normalized by the dynamic pressure $q_\infty = 1/2\gamma P_\infty M_\infty^2$. This kind of representation allows to educe convective features denoted by an inclined contour pattern and to show that the pressure fluctuations are the most energetic in the reattachment region. This corroborates the high broadly distributed rms pressure levels near the reattachment (see figure 7). Indeed, it has been shown in earlier studies (see for instance Cherry *et al.*[45], Kiya and Sasaki[76], Lee and Sung[77]) that the instantaneous negative peaks are associated with the passage of large-scale vortices while positive peaks are related to free-stream inrush between the vortices. This figure also highlights the occurrence of upstream (respectively downstream) propagating disturbances denoted by an inclined contour pattern with negative (respectively positive) slope. The change in the direction of propagation of the most energetic disturbances near the middle of the circulating zone are worth being noticed. This important feature is similar to what Hudy *et al.*[54] observed in the reattachment region downstream of a fence. These authors got interested in the phase of the pressure signals

and observed a phase-angle jump of about π near the center of the recirculating bubble.

To evaluate the velocity of the propagating disturbances, one may compute the frequency wave number spectrum (f-k). The corresponding estimator $\Psi(f,k)$ is based on the cross spectrum $S_{x_i x_j}(f)$ of space-time wall pressure signal between points x_i and x_j:

$$\Psi(f,k) = P(k)^H M(f) P(k) \tag{11}$$

where H denotes the Hermitian transpose and the interspectral matrix M and P are respectively defined by:

$$\begin{aligned} M_{ij}(f) &= S_{x_i x_j}(f) \\ P_i(k) &= e^{-\left(\sqrt{-1}kx_i\right)} \end{aligned} \tag{12}$$

The main interest of this estimator is that it allows to investigate non-equally spaced sensors while a two-dimensional Fourier transform requires equally spaced sensors. Moreover, the frequency wave-number spectrum enables to evidence multiple convection velocities while phase data are inevitably contaminated by wave numbers that may not contribute to the advective motion.

Figure 17 presents the computed frequency wave-number spectrum for respectively the points located in the first half-part of the recirculation zone (i.e. $X/L_r \leq 0.5$), points located in the second half-part and finally for all the investigated sensors. This allows (see Hudy *et al.*[54]) to determine more accurately the upstream and downstream propagating disturbances. At positive wave numbers, one obtains a downstream propagating velocity $U_c = 0.6U_\infty$ which from $U_c = 2\pi/(\Delta k_x/\Delta f)$ where $\Delta k_x/\Delta f$ is the slope of the line characterizing the convection speed. This convection velocity corresponds to the shear layer structures signature at the wall (see Refs.[45,47]).

At negative wave numbers, an upstream convective velocity of $U_c = 0.26U_\infty$ is depicted. Note that this upstream propagating velocity is not evidenced in the spectrum for the sensors located at $X/L_r \geq 0.5$. This important feature also stressed by Hudy *et al.*[54] provides evidence that the most energetic upstream propagating disturbances are confined in the range $X/L_r \leq 0.5$. In the case of a backward-facing step, Heenan and Morrison[78] also found from cross correlation, a negative convection as well as a positive convection in the recirculation region close to the step. However, evidence of this upstream convection has not been reported systematically (see Farabee and Casarella[79] and Lee and Sung[52]). These

latter authors performed multi-point pressure measurements downstream a backward-facing step and computed a frequency wave number spectrum similar to the one in figure 17. They found a stationary spatial mode ($k_x = 0$) that they associated to the flapping motion while no upstream convection velocity was depicted.

Hudy *et al.*[54] remind that the process associating upstream and downstream travelling disturbances originating from a common source in the middle of the recirculation zone indicate the possible existence of an absolutely unstable flow region. Let us briefly recall that a flow is termed convectively unstable if the disturbances grow in space, convecting away from the source, whereas it is called absolutely unstable if the disturbances grow in time and spread everywhere.

Wee *et al.*[80] argued that the eddy shedding phenomena are due to inviscid characteristics of the mean velocity profile. Then, they conducted a local stability analysis of a family of velocity profiles issued either from a composite hyperbolic tangent function or a numerical simulation in the context of a separating shear flow downstream of a two-dimensional backward facing step of height H. They showed that the largest growth rate of an absolute instability is located near the middle of the recirculation and that the growth rate of the absolute unstable mode is controlled by the amount of backflow. This important result is also supported by the findings of Heenan and Morrison[78]. These authors used a porous wall in the vicinity of the reattachment region to diminish significantly the amount of backflow within the recirculation area. They observed that this weakening of the amount of backflow resulted in a quasi-cancellation of the flow frequency peak associated with the shear layer flapping and that the upstream convection motion discussed previously was removed.

Nevertheless, it is not clear whether the absolute instability is associated with vortex shedding or shear-layer flapping. Indeed, Wee *et al.*[80] showed that the corresponding frequency of the absolute instability mode is determined as $St_H = fH/U_\infty = O(0.1)$ ($St_H = 0.067$ in their case) while Hudy *et al.*[54] suggest the existence of an absolute instability at a lower frequency of $fH/U_\infty = O(0.01)$ which is commonly attributed the shear-layer flapping. Driver *et al.*[81] noted in their backward facing step flow that it was not possible to define precisely a frequency which separates the flapping motion from that of a vortical structure. Let us recall that the self-sustained motion in our axisymmetric afterbody is observed at $St_H = St_D.H/D \approx 0.06$ which is in accordance with the findings of Wee *et al.* in the case of a two-dimensional backward facing step flow. Nevertheless, the occurrence of cyclic motion

concerning the secondary corner vortex at $St_H = St_D.H/D \approx 0.08$ suggests there different aspect of the same motion may be involved.

VII. CONCLUSION

Numerical simulations have been carried out on a compressible axisymmetric step flow for a Reynolds number based on the diameter of the body nearly equal to $1.1\,10^6$. The literature review has revealed that less attention was paid to the analysis of an axisymmetric separating/reattaching flow than to its two-dimensional counterpart. The Reynolds averaged data have been firstly compared with the available experimental data and with those of classical backward facing step flows. It has been shown that this axisymmetric step configuration shares many similar features with two-dimensional facing step flows as regards the shear layer instability process and especially its strong growth rate. The maximum of pressure fluctuations reaches a plateau just upstream of the mean shear layer reattachment location $(Cp_{rms})_{max} \approx 0.05 - 0.06$.

The spectral analysis of the pressure fluctuations has shown different frequency contributions depending on the location considered in the recirculation bubble. Close to the step, the spectrum displays a peak near a normalized frequency $f.L_r/U_\infty \approx 0.08$ which has been shown to represent the footprint of the vertical motion of the bubble (often called shear layer flapping). Unlike experiment, calculation provides the whole aerodynamic field and allows in particular a deep analysis of the unsteady field. Through flow visualizations, it has been shown that the reattachment length moves over a distance up to 30% of the mean reattachment length whose characteristic frequencies is given by $f.L_r/U_\infty \approx 0.2$. Besides, it has been observed that the secondary corner vortex experiences a cycle of growth and decay. The correspondence between the frequencies of this secondary corner vortex dynamics and the flapping motion suggests that there should be different aspects of the same motion. In addition, it has been shown that the most contributing spatial length in the azimuthal direction to the energy involves two-points diametrically opposite and that frequencies $f.L_r/U_\infty \approx 0.08$ and 0.2 are strongly dominated by the antisymmetric mode $m = 1$, although the flow is axisymmetric in a time-averaged sense. Theses results show that there is an ordered structure in this axisymmetric separating/reattaching flow dominated

by large scale coherent motions. As stressed by Fuchs *et al.*[16], these large scale coherent structures are more than just an interesting phenomenon since only anti-symmetric fluctuations associated with the $m = 1$ mode contribute to the lateral force acting on the rearbody.

Finally, possible onsets of large-scale self-sustained motions of the separated area have been discussed. We are inclined to rule out the hypothesis of aero-acoustic feedback process between the separation and reattachment points. Indeed, the space-time characteristics of wall-pressure fluctuations on the emerging body feature strong feedback disturbances originating from the center of the recirculating bubble rather than from the reattachment point. Frequency/wave-number spectrum analysis shows that the most energetic upstream propagating disturbances are confined in the range $X/L_r \leq 0.5$. Although evidence of this upstream convection has not been reported systematically, the present axisymmetric flow shares this characteristic feature observed by Heenan and Morrison[78]and Hudy *et al.*[54]. These latter authors reminded that the process associating upstream and downstream travelling disturbances originating from a common source in the middle of the recirculation zone indicate the possible existence of an absolutely unstable flow region. A rigorous approach to this aspect would consists in a global linear analysis of this compressible axisymmetric step flow and will follow the present work.

a. Acknowledgments

The authors are greatly indebted to MM. Deprés and Reijasse from ONERA for supplying the experimental data and to their colleagues MM. Dandois and Simon from ONERA for fruitful discussions. M. Lambare from CNES is warmly acknowledged for his support and many stimulating discussions on launcher buffet loads. The authors also wish to thank all the people involved in the past and present evolution of the FLU3M code. This study is partly funded by CNES within the framework of the CNES Research and Technology Program ATAC (Aerodynamics of nozzles and afterbodies) under technical cooperation between CNES/ONERA/CNRS/SNECMA and EADS-LV.

---

* Electronic address: `sebastien.deck@onera.fr`

[1] D. Deprés, P. Reijasse, and J.P. Dussauge. Analysis of Unsteadiness in Afterbody Transonic

Flows. *AIAA J. ,vol 42, No. 12, pp 2541-2550*, 2004.

[2] R.H. Coe. Steady and fluctuating pressures at transonic speeds on hammerhead launch vehicles. *NASA, Technical Memorandum TMX-778, December*, 1962.

[3] D.G. Mabey. Some measurements on base pressure fluctuations at subsonic and supersonic speeds. *Aeronautical Research Council, ARC-CP-1204; also Royal Aircraft Establishment, RAE-TR-70148, Bedford (UK), Aug.1970*, 1972.

[5] H. Wong, J. Meijer, and R. Schwane. Experimental and Theoretical Investigation of Base-Flow Buffeting on Ariane 5 Launch Vehicles. *AIAA Journal of Propulsion and Power, Vol.23, No. 1, pp 116-122*, 2007.

[4] S. Deck, E. Garnier, and P. Guillen. Turbulence modelling applied to space launcher configurations. *Journal of Turbulence, vol.3, (57), pp 1-21*, 2002.

[6] A. Roshko. On the wake and drag of bludd bodies. *J. Aero. Sci., vol 22, pp 124-132*, 1955.

[7] J.R. Calvert. Experiments on low speed flow past cones. *Journal of Fluid Mechanics, vol.27, part 2, pp 273-289*, 1966.

[8] J.F. Nash, V.G. Quincey, and J. Callinan. Experiments on two-dimensional base flow at subsonic and transonic speeds. *Aeronautical Research Council, Tech. Report RM 3427, Jan.*, 1963.

[9] S.L. Gai and S.R. Patil. Subsonic Axisymmetric Base Flow Experiments with base Modifications. *Journal of Spacecraft, vol.17, No.1, pp 42-46*, 1980.

[10] J. Délery and M. Siriex. Base flows behind missiles. *Tech. Rept, AGARD LS-98*, 1979.

[11] S. Taneda. Visual observationss of the flow past a sphere at retnolds numbers between 10^4 and 10^6. *Journal of Fluid Mechanics, vol 85, pp 187-192*, 1978.

[12] E. Berger, D. Scholz, and M. Schumm. Coherent vortex structures in the wake of a sphere and a circular disk at rest and underforced vibrations. *Journal of Fluid Structures, vol 4, pp 231-257*, 1990.

[13] G. Constantinescu and K. Squires. Numerical investigations of flow over a sphere in the subcritical and supercritical regimes. *Physics of Fluids, vol.16, No.5 , pp 1449-1466*, 2004.

[14] P. Spalart, W.H. Jou, M. Stretlets, and S.R. Allmaras. Comments on the feasibility of LES for wings and on a hybrid RANS/LES approach. *In Proceedings pp 137-147, 1st AFSOR Int. Conf. on DNS/LES, Ruston*, 1998.

[15] H. Higuchi. Visual Study on Wakes Behind Solid and Slotted Axisymmetric Bluff Bodies. *Journal of Aircraft, vol.28, No.7, pp 427-430*, 1991.

[16] H.V. Fuchs, Mercker E., and U. Michel. Large scale coherent structures in the wake of axisymmetric bodies. *Journal of Fluid Mechanics, vol 93, part 1, pp 185-207*, 1979.

[17] K.M. Eldred. Base pressure fluctuations. *Journal of the Acoustical Society of America, vol.33, No.1, pp 59-63*, 1961.

[18] J.P. Flodrops and J.M. Desse. Sillage d'un culot axisymétrique. *Onera/IMFL, Techn. Rept No.85/19, April*, 1985.

[19] R.A. Merz, R.H. Page, and C.E.G. Przirembel. Subsonic Axisymmetric near-Wake Studies. *AIAA J. vol.16, No.7, pp 656-662*, 1978.

[20] M. Alam and N.D. Sandham. Direct numerical simulation of short laminar separation bubbles with turbulent reattachment. *Journal of Fluid Mechanics, vol 403, pp 223-250*, 2000.

[21] P.A. Monkewitz. A note on vortex shedding from axisymmetric bluff bodies. *Journal of Fluid Mechanics, vol.192, pp 561-575*, 1988.

[22] A. Weickgenannt and P.A. Monkewitz. Control of vortex shedding in an axisymmetric. *Eur.J. Mech. B-Fluids, vol 19, pp 789-812*, 2000.

[23] A. Sevilla and C. Martinéz-Bazân. Vortex shedding in high reynolds number axisymmetric bluff-body wakes: Local linear instability and global bleed control. *Physics of Fluids, vol.16, No.9 , pp 3460-3469*, 2004.

[24] P.W. Bearman. The effect of base bleed on the flow behind a two-dimensional model with a blunt trailing edge. *Aero. Quart, vol 18, pp 207-224, August*, 1967.

[25] F. Motallebi and J.F. Norbury. The effect of base bleed on vortex shedding and base pressure in compressible flow. *Journal of Fluid Mechanics, vol 110, pp 273-292*, 1981.

[26] P.W. Bearman. Investigation of the flow behind a two-dimensionnal model with a blunt trailing edge and fitted with splitter plates. *Journal of Fluid Mechanics, vol 21, part 2, pp 241-255*, 1965.

[27] J.K. Eaton and J.P. Johnston. A Review of Research on Subsonic Turbulent Flow Reattachment. *AIAA J., vol.19, No.9, pp 1093-1100, September*, 1981.

[28] P. Bradshaw and F.Y.F. Wong. Reattachment of a turbulent boundary layer. *Journal of Fluid Mechanics, vol.52, part 1, pp 113-135*, 1972.

[29] D.G. Mabey. Analysis and Correlation of Data on Pressure Fluctuations in Separated Flow. *Journal of Aircraft, vol.9, No.9, pp 642-645*, 1972.

[30] L.W. Sigurdson. The structure and control of a turbulent reattaching flow. *Journal of Fluid*

Mechanics, vol.298, pp 139-165, 1995.

[31] M. Péchier, Ph. Guillen, and R. Caysac. Magnus Effect Over Finned Projectiles. *AIAA Journal of Spacecraft and Rockets, vol.38, No.4, pp. 542-549*, 2001.

[32] S. Deck, Ph. Duveau, P. d'Espiney, and Ph. Guillen. Development and application of Spalart Allmaras one equation turbulence model to three-dimensional supersonic complex configurations. *Aerospace Science and Technology, Vol. 6, No. 3, pp 171-183*, 2002.

[33] I. Mary and P. Sagaut. Large eddy simulation of flow around an airfoil near stall. *AIAA J., vol.40, No.6, pp 1139-1145*, 2002.

[34] L. Larchevêque, O. Labbé, I. Mary, and P. Sagaut. Les of a compressible flow past a deep cavity. *Physics of Fluids, vol.15, No.1 , pp 193-210*, 2003.

[35] J. Dandois, E. Garnier, and P. Sagaut. Unsteady Simulation of Synthetic Jet in a Crossflow. *AIAA J. vol.44, No.2, pp 225-238*, 2006.

[36] S. Deck. Zonal-Detached Eddy Simulation of the Flow around a High-Lift Configuration. *AIAA Journal, vol 43., No. 11, pp 2372-2384*, 2005.

[37] P.R. Spalart, S. Deck, M.L Shur, K.D. Squires, M. Strelets, and A. Travin. A New Version of Detached-Eddy Simulation, Resistant to Ambiguous Grid Densities. *Theoretical and Computational Fluid Dynamics, Vol 20, pp 181-195, July 2006*, 2006.

[38] P. Sagaut, S. Deck, and M. Terracol. Multiscale and Multiresolution Approaches in Turbulence. *Imperial College Press, 356 pages*, 2006.

[39] S. Deck. Detached Eddy Simulation of transonic buffet over a supercritical airfoil. *AIAA Paper 04-5378, 22nd AIAA Applied Aerodynamics Conference, Providence, Rhode Island, August*, 2004.

[40] F. Simon, S. Deck, Ph. Guillen, and P. Sagaut. Reynolds Averaged Navier Stokes / Large Eddy Simulations of supersonic base flow. *AIAA J., vol.44, No. 11, pp 2578-2590*, 2006.

[41] D. Deprés. *Analyse physique et modélisation des instationnarités dans les écoulements d'arrière-corps transoniques*. PhD thesis, Université de la Méditerranée Aix-Marseille II, 2003.

[42] Delcayre F. Dubief Y. On coherent-vortex identification in turbulence. *Journal of turbulence, vol. 1, (11)*, 2000.

[43] Z.D. Husain and A.K.M.F. Hussain. Axisymmetric Mixing Layer: Influence of he Initial and Boundary Conditions. *AIAA J. vol.17, No.1, pp 48-55*, 1979.

[44] C.M. Ho and L.S. Huang. Subharmonics and vortex merging in mixing layers. *Journal of Fluid*

Mechanics, vol.119, pp 443-473, 1982.

[45] N.J. Cherry, R. Hillier, and M.E.M.P. Latour. Unsteady measurements in a separated and reattaching flow. *Journal of Fluid Mechanics, vol.144, pp 13-46*, 1984.

[46] I.P. Castro and A. Haque. The structure of a turbulent shear layer bounding a separation region. *Journal of Fluid Mechanics, vol.179, pp 439-468*, 1987.

[47] J. Dandois, E. Garnier, and P. Sagaut. Dns/les of active separation control. *Accepted for publication in Journal of Fluid Mechanics*, 2006.

[48] L. Larchevêque, P. Sagaut, T.H. Le, and P. Compte. Large-eddy simulation of a compressible flow in a three-dimensional open cavity at high reynolds number. *Journal of Fluid Mechanics, vol 516, pp 265-301*, 2004.

[49] S. Jovic. An experimental study of separated/reattached flow behind a backward-facing step. $re_h = 37000$. *NASA, Technical Memorandum 110384*, 1996.

[50] C. Chandrsuda and P. Bradshaw. Turbulence structure of a reattaching mixing layer. *Journal of Fluid Mechanics, vol 110, pp 171-194*, 1981.

[51] D.M. Driver, H.L. Seegmiller, and J. Marvin. Time-dependent bahavior of a reattaching shear layer. *AIAA J. vol.25, No.7, pp 914-919*, 1987.

[52] I. Lee and H.J. Sung. Characteristics of wall pressure fluctuations in separated and reattaching flows over a backward facing step. Part I: Time-mean statistics and cross-spectral analyses. *Experiments Fluids, vol.30, pp 262-272*, 2001.

[53] T.H.H. Lê. *Etude expérimentale du couplage entre l'écoulement transonique d'arrière-corps et les charges latérales dans les tuyères propulsives.* PhD thesis, University of Poitiers, Dpt of Engineering Sciences, 2005.

[54] L.M. Hudy, A.M. Naguib, and W.M. Hunphreys. Wall-pressure-array measurements beneath a separating/reattaching flow region. *Physics of Fluids, vol.15, No.3 , pp 706-717*, 2003.

[55] R.H. Coe. The effects of some variations in launch-vehicle nose shape on steady and fluctuating pressures. *NASA, Technical Memorandum TMX-636, March*, 1962.

[56] R. Kumar, P.R. Viswanath, and A. Prabhu. Mean and Fluctuating Pressure in Boat-Tail Separated Flows at Transonic Speeds. *AIAA Journal of Spacecraft and Rockets, vol.39, No.3, pp 430-438, May-June*, 2002.

[57] D.G. Mabey. Pressure fluctuations caused by separated bubble flows at subsonic speeds. *Royal Aircraft Establishment, Tech. Report RAE-TR-71160, Aug.*, 1971.

[58] J.S. Bendat and A.G. Piersol. Random data: Analysis and measurements procedures. *Wiley-Interscience, New-York*, 1971.

[59] P. Huerre and M. Rossi. Hydrodynamic instabilities in open flows. *In : Hydrodynamics and nonlinear instabilities. Ed C. Godrèche and P. Manneville, pp 81-214. Cambridge University Press.*, 1998.

[60] S. Deck and A.T. Nguyen. Unsteady Side Loads in a Thrust Optimized Contour Nozzle at Hysteresis regime. *AIAA Journal, vol.42, No.9, pp 1878-1888*, 2004.

[61] S. Deck and E. Garnier. Detached and Large Eddy Simulation of unsteady side-loads over an axisymmetric afterbody. *In proceedings* 5^{th} *European Symposium on Aerothermodynamics for Space Vehicles, pp 297-304, Cologne, Germany, 8-11 november*, 2004.

[62] S.W. Pronchick and S.J. Kline. An experimental investigation of the structure of a turbulent reattaching flow behind a backward-facing step. *Stanford University. Thermoscience Div. Rep. MD-42, June*, 1983.

[63] R.L. Simpson. Turbulent boundary layer separation. *Annual Review of Fluid Mechanics, 21:205-234*, 1989.

[64] S.D. Hall, M. Behnia, C.A.J. Fletcher, and G.L. Morrison. Investigation of the secondary corner vortex in a benchmark turbulent backward-facing step using cross-correlation particle imaging velocimetry. *Experiments Fluids, vol.35, pp 139-151*, 2003.

[65] P.G. Spazzini, G. Iuso, M. Onorato, N. Zurlo, and G.M. Di Cicca. Unsteady behavior of back-facing flow. *Experiments Fluids, vol.30, pp 551-561*, 2001.

[66] J.M. Chomaz, P. Huerre, and L.G. Redekopp. Biffurcation to Local and Global Modes in Spatially Developping Flows. *Physical Review Letters, Vol.60, No. 1, pp 25-28*, 1988.

[67] N. Forestier, L. Jacquin, and P. Geffroy. The mixing layer over a deep cavity at high subsonic speed. *Journal of Fluid Mechanics, vol 475, pp 101-145*, 2003.

[68] B.H.K. Lee. Transsonic buffet on a supercritical airfoil. *Aeronautical Journal, pp 143-152*, 1990.

[69] S. Deck. Numerical simulation of transonic buffet over a supercritical airfoil. *AIAA J., vol 43., No. 7, pp 1556-1566*, 2005.

[70] P. Huerre and P.A. Monkewitz. Local and global instabilities in spatially developping flows. *Annual Review of Fluid Mechanics, 22:473*, 1990.

[71] C.K.W. Tam. Discrete Tones of Isolated Airfoils. *Journal of the Acoustical Society of America, vol.55, No.6, pp 1173-1177*, 1974.

[72] D. Rockwell. Oscillations of Impinging Shear Layers. *AIAA J., vol.21, No.5, pp 645-664*, 1983.

[73] D. Rockwell and E. Naudasher. Self-sustained oscillations of impinging free shear layers. *Annual Review of Fluid Mechanics, 11:67-94*, 1979.

[74] C.M. Ho and N.S. Nosseir. Dynamics of an impinging jet. part 1. the feedback phenomenon. *Journal of Fluid Mechanics, vol.105, pp 119-142*, 1981.

[75] M. Kiya, M. Shimizu, and O. Mochizuki. Sinusoïdal forcing of a turbulent separation bubble. *Journal of Fluid Mechanics, vol 342, pp 119-139*, 1997.

[76] M. Kiya and M. Sasaki. Structure of large-scale vortives and unsteady reverse flow in the reattaching zone of a turbulent separation bubble. *Journal of Fluid Mechanics, vol 154, pp 493-491*, 1985.

[77] I. Lee and H.J. Sung. Multiple-arrayed pressure measurement for investigation of the unsteady flow structure of a reattaching shear layer. *Journal of Fluid Mechanics, vol 463, pp 377-402*, 2002.

[78] A.F. Heenan and Morrison J.F. Passive control of pressure fluctuations generated by separated flows. *AIAA J. vol.36, No.6, pp 1014-1022*, 1998.

[79] T.M. Farabee and M.J. Casarella. Measurements of Fluctuating Wall Pressure for Separated/Reattached Boundary Layer Flows. *Experiments Fluids, vol.108, pp 301-307*, 1986.

[80] D. Wee, T. Yi, A. Annaswamy, and A.F. Ghoniem. Self-sustained oscillations and vortex shedding in backward-facing step flows: Simulation and linear instability analysis. *Physics of Fluids, vol.16,No. 9, pp 3361-3373*, 2004.

[81] D.M. Driver, H.L. Seegmiller, and J. Marvin. Unsteady Behavior of a Reattaching Shear layer. *aiaa paper 83-1712, 16th AIAA Fluid and Plasma Dynamics Conference, Danvers, Massachusetts, July*, 1983.

[82] E. Achenbach. Vortex shedding from spheres. *Journal of Fluid Mechanics, vol 62, pp 209-221*, 1974.

[83] R. A. Merz. Subsonic Base Pressure Fluctuations. *AIAA Journal, Vol. 17, No. 4*, 1979.

[84] J. L. Herrin and J. C. Dutton. Supersonic Base Flow Experiments in the Near Wake of a Cylindrical Afterbody . *AIAA Journal, Vol. 32, No. 1, pp. 77-83*, 1994.

[85] J. R. Janssen and J. C. Dutton. Time-Series Analysis of Supersonic Base-Pressure Fluctuations. *AIAA Journal, Vol. 42, No. 3, pp.605-613*, 2004.

[86] J. Tihon, J. Legrand, and P. Legentilhomme. Near-wall investigation of backward facing step

flows. *Experiments Fluids, vol.31, pp 484-493*, 2001.

[87] W.J. Devenport and E.P. Sutton. Near-Wall Bahavior of Separated and Reattahing Flows. *AIAA Journal, vol.29, No.1, pp 25-31*, 1991.

[88] A. Roshko and G.J. Thomke. Observations of Turbulent Reattachment behind an axisymmetric Downstream-Facing Step in Supersonic Flow. *AIAA J., vol.4, No.6, pp 975-980*, 1966.

[89] S.G. Goebel and J.G. Dutton. Experimental study of compressible turbulent mixing layers. *AIAA J. vol.29, No. 4, pp 538-546*, 1990.

[90] J.B. Freund, S.K. Lele, and P. Moin. Compressibility effects in a turbulent annular mixing layer. part i: Turbulence and growth rate. *Journal of Fluid Mechanics, vol.421, pp 229-267*, 2000.

Figures

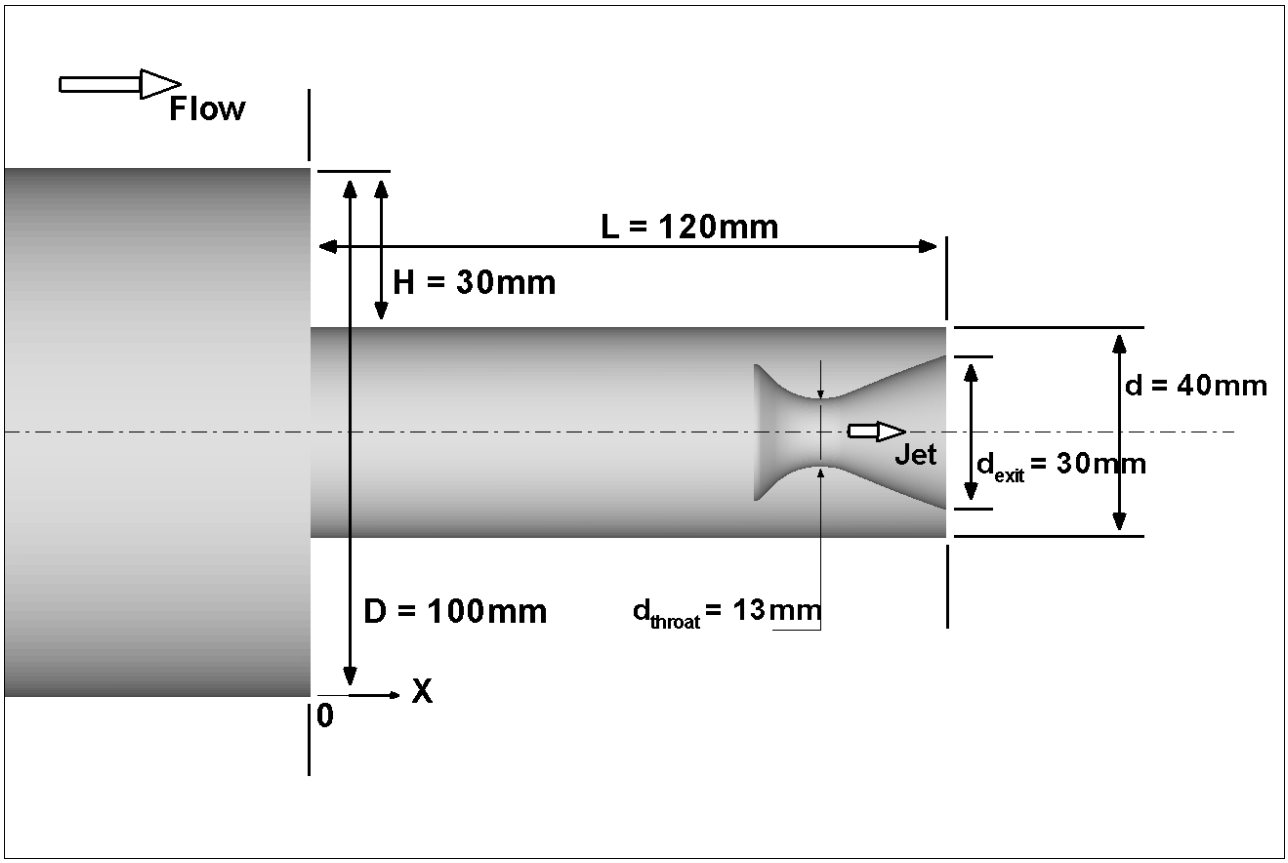

FIG. 1: Schematic of the axisymmetric afterbody model.

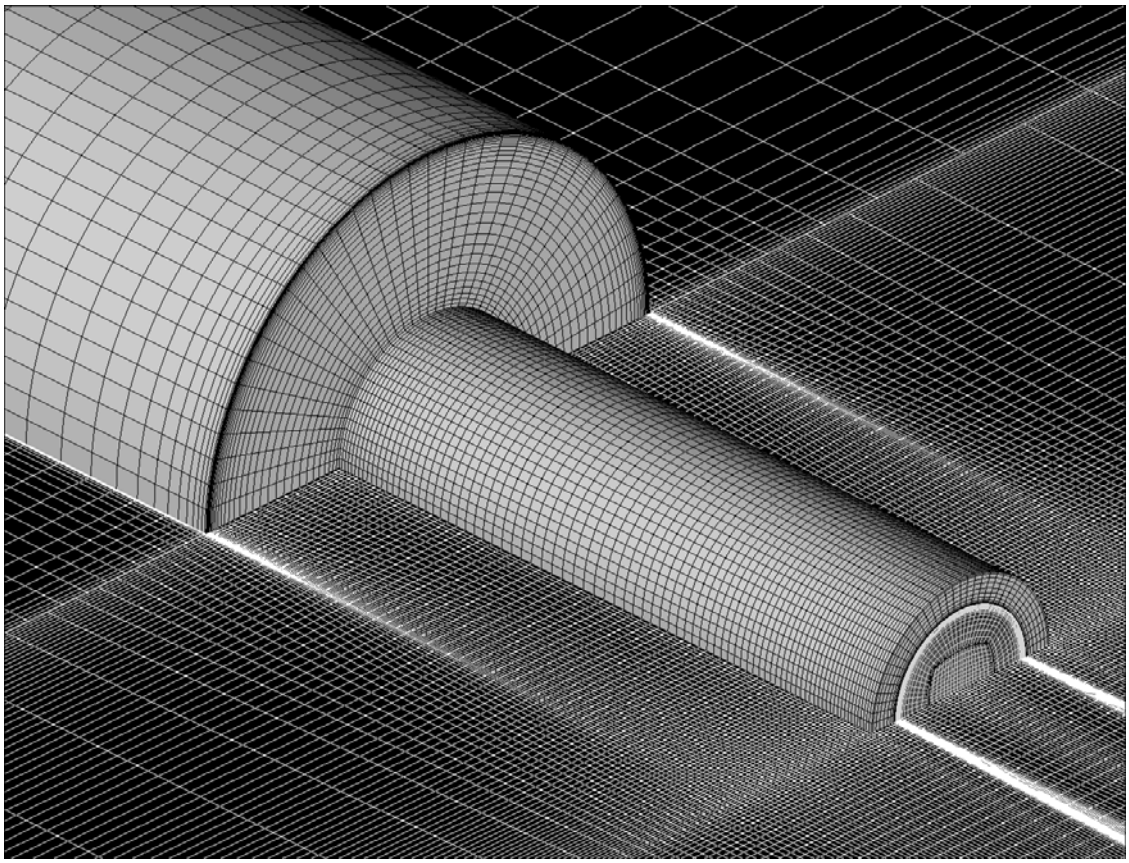

FIG. 2: Cut-away through the 3D mesh (M3 grid) around the afterbody (only one cell over two are plotted in each direction).

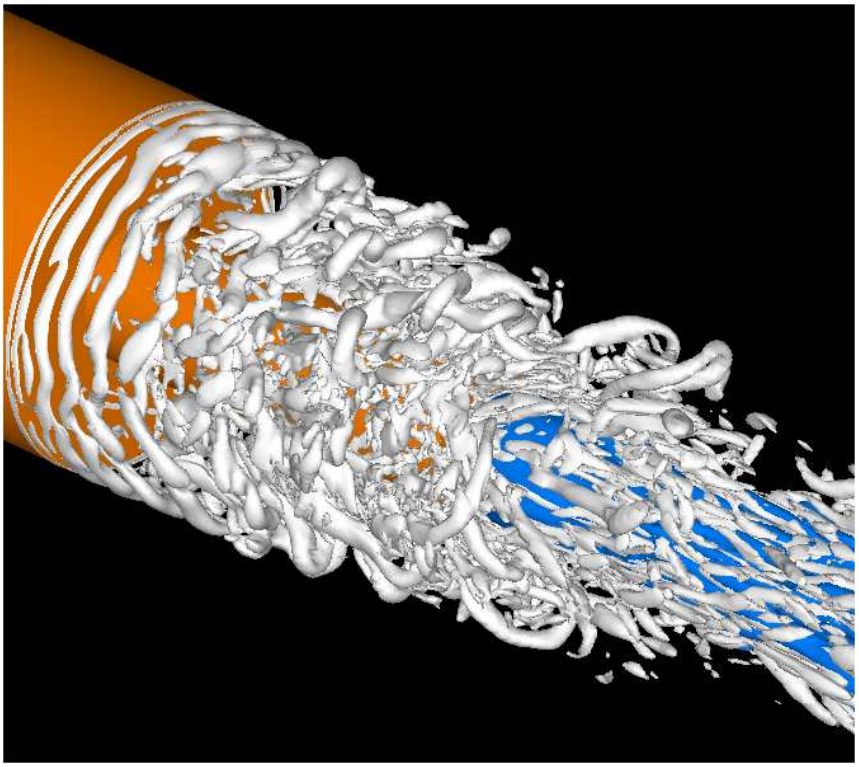

FIG. 3: Coherent structures downstream of the axisymmetric step flow educed using iso-surface of $\frac{QU_\infty^2}{D^2} = 70$.

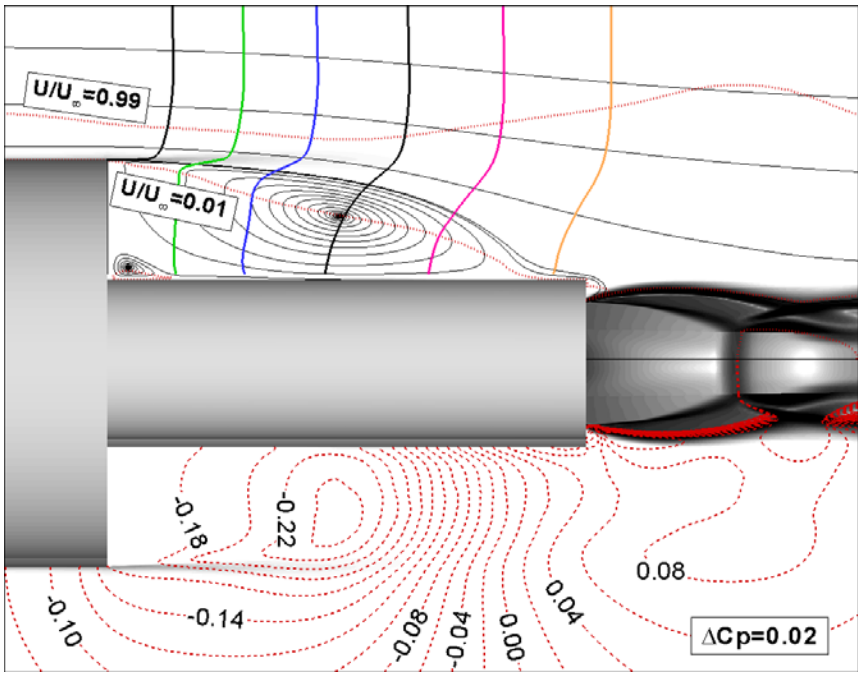

FIG. 4: Time-averaged flowfield. Upper-part: velocity profiles and iso-velocity (dotted) line $U/U_\infty = 0.01 - 0.99$. Lower part: iso-Cp (dashed) lines with $\Delta Cp = 0.02$ between two lines.

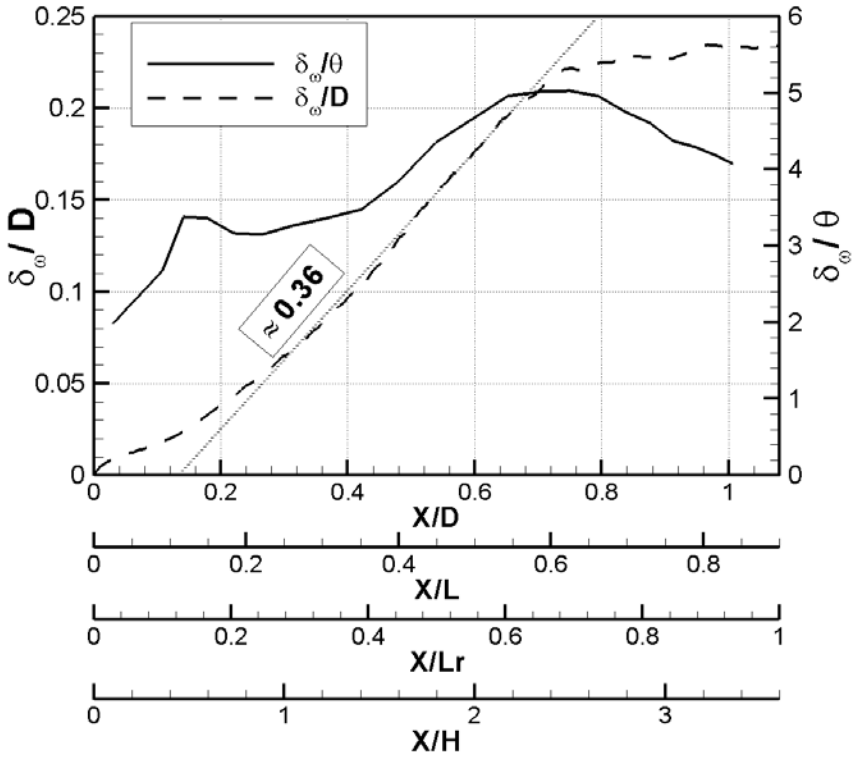

FIG. 5: Vorticity thickness and ratio between vorticity and momentum thicknesses along the mixing layer.

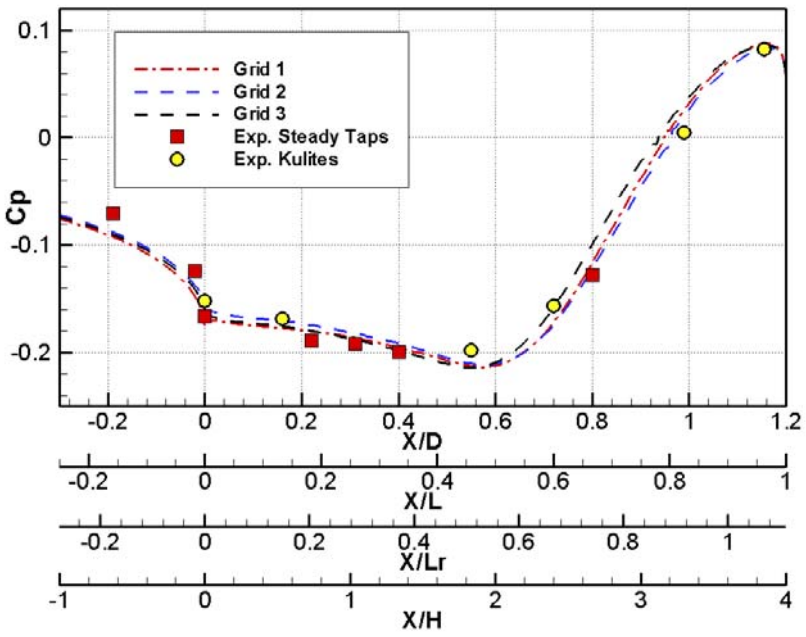

FIG. 6: Streamwise distribution of the pressure coefficient.

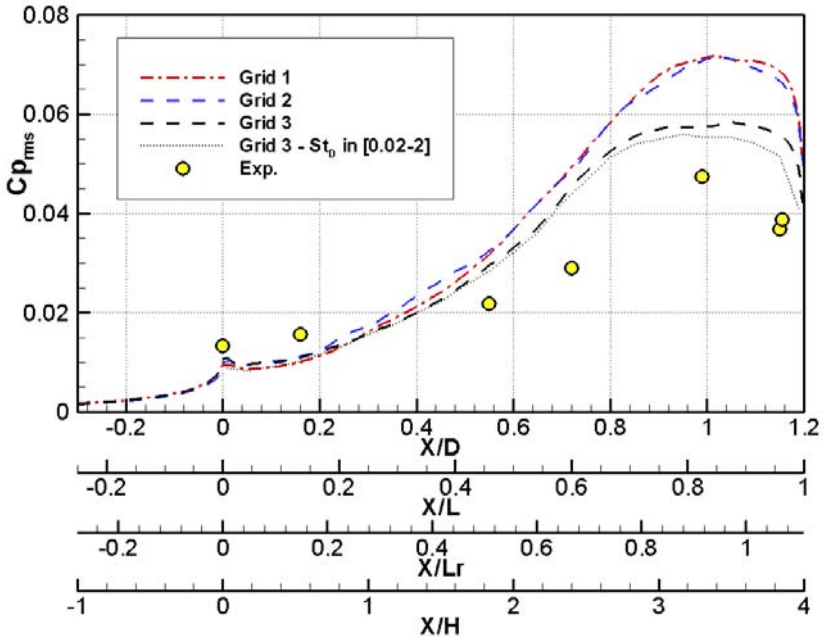

FIG. 7: Streamwise distribution of the coefficient of rms pressure fluctuations.

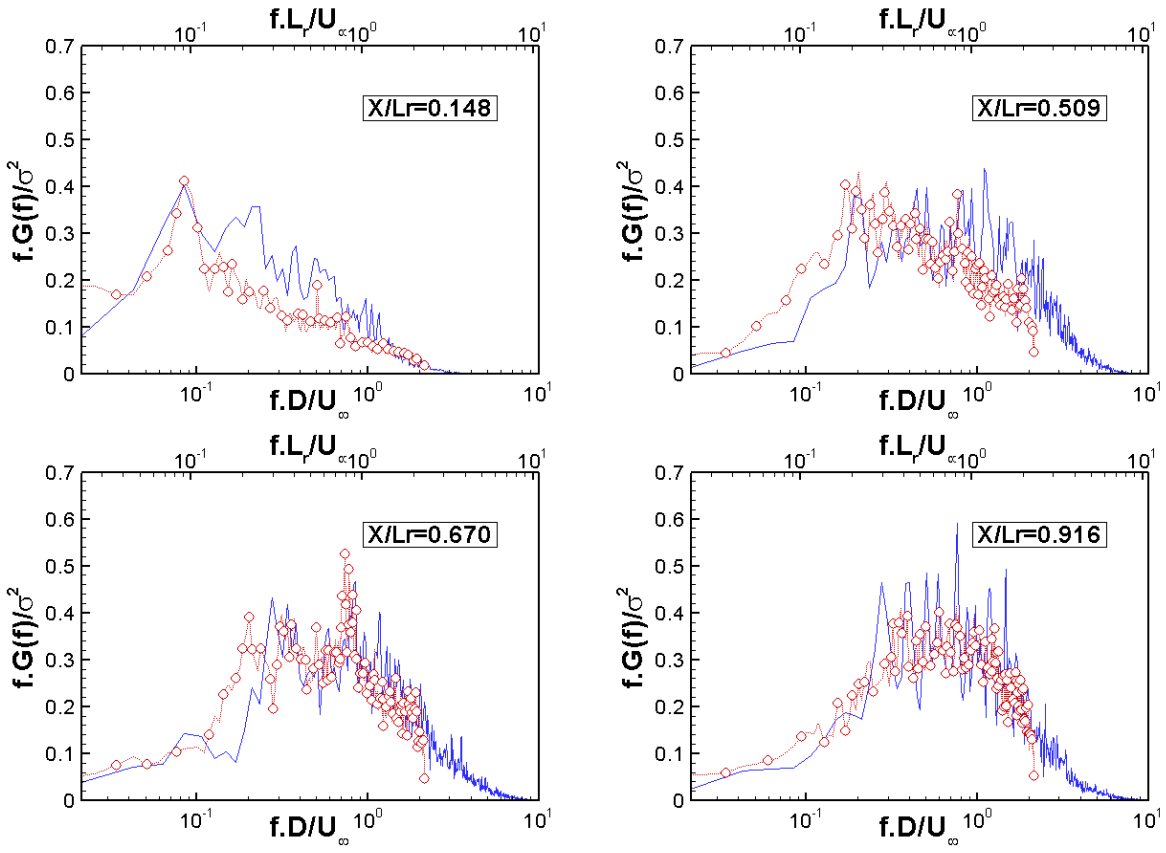

FIG. 8: Pressure spectra along the step. *.o.*, Exp.; ___ , Calc.

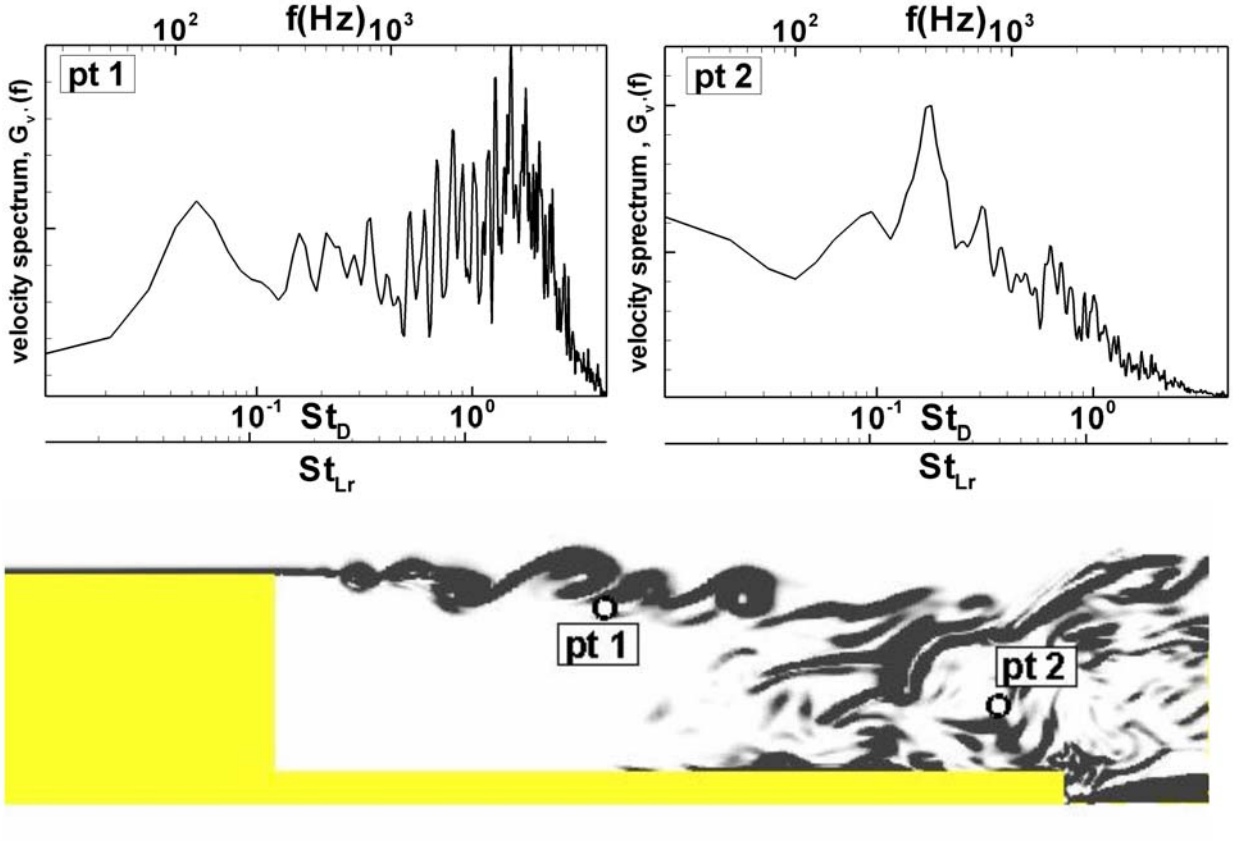

FIG. 9: Velocity spectra along the mixing layer.

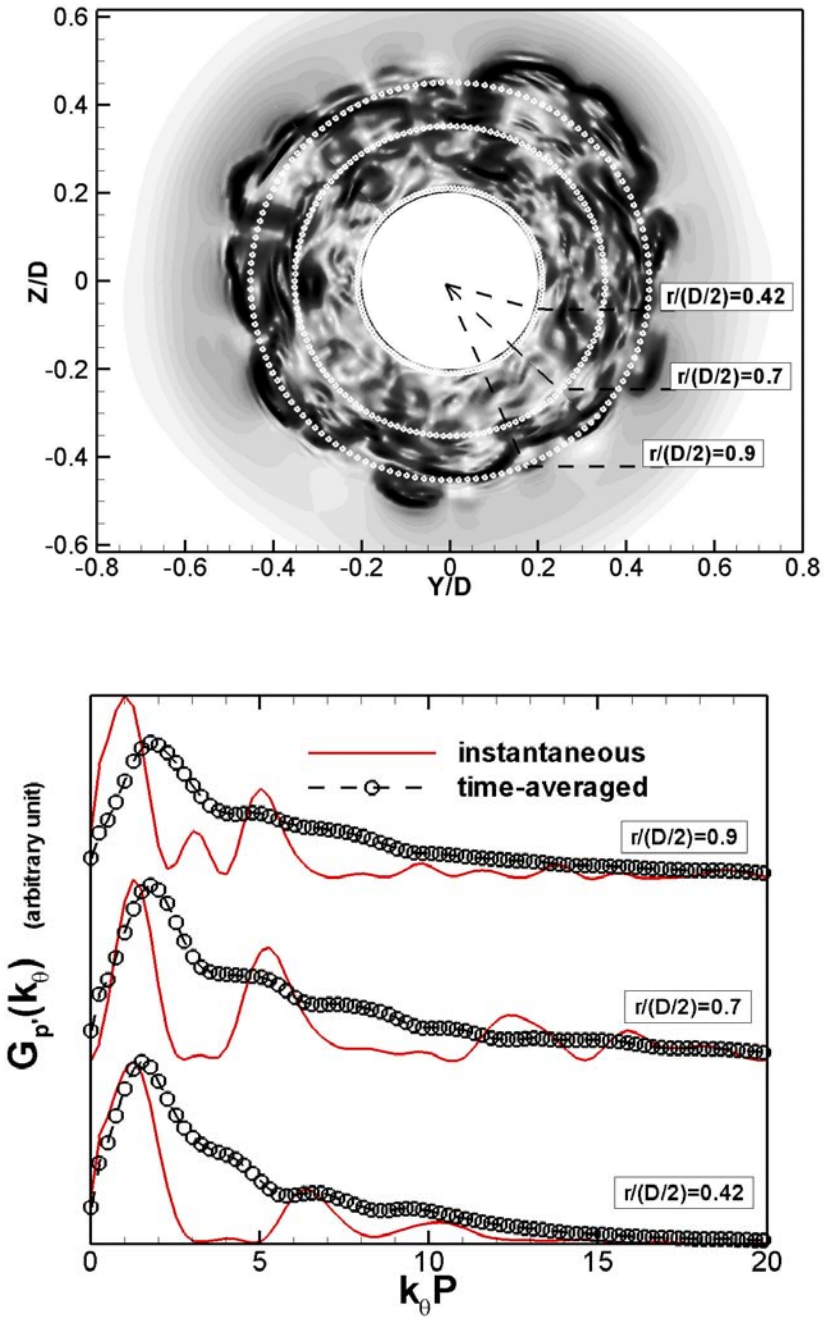

FIG. 10: Upper-part: instantaneous schlieren at $X/L_r = 0.670$ showing the location of each crown of sensors. Lower part: spectrum of pressure fluctuation in azimuthal wave-number space at $X/L_r = 0.670$.

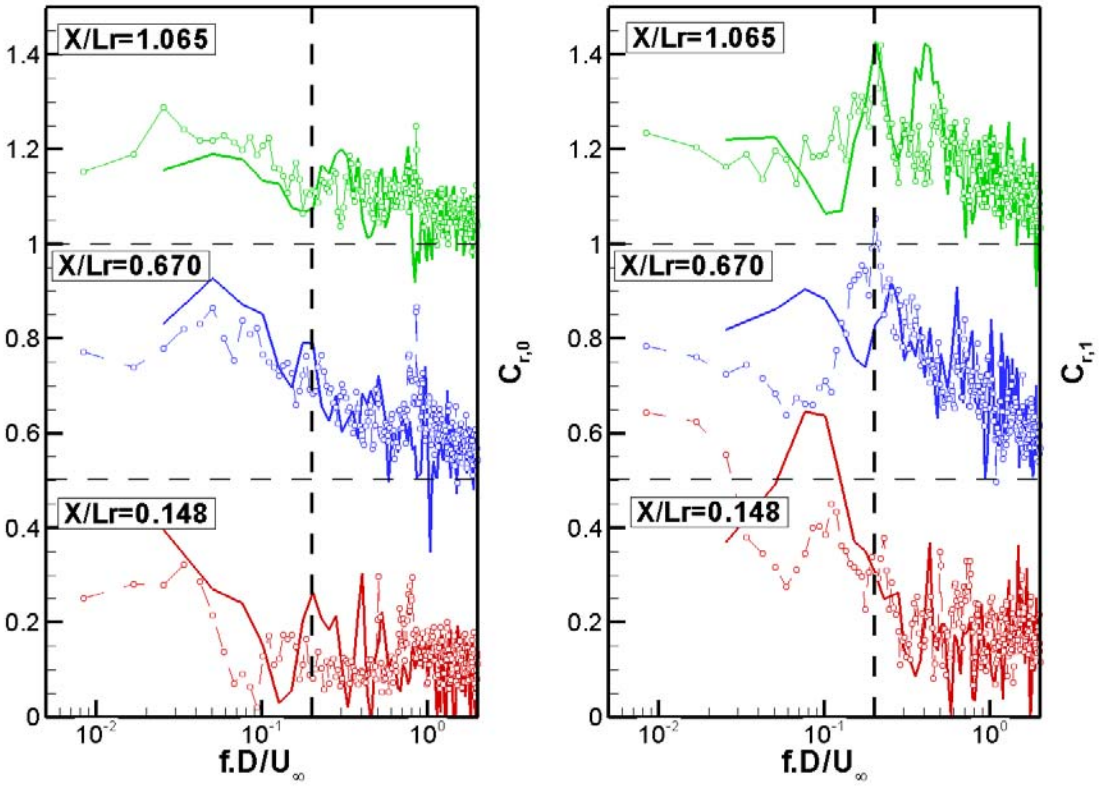

FIG. 11: Spectra of the two first azimuthal pressure modes $C_{r,0}$ and $C_{r,1}$ for three streamwise locations. $-o-$, Exp.; ___ , Calc.

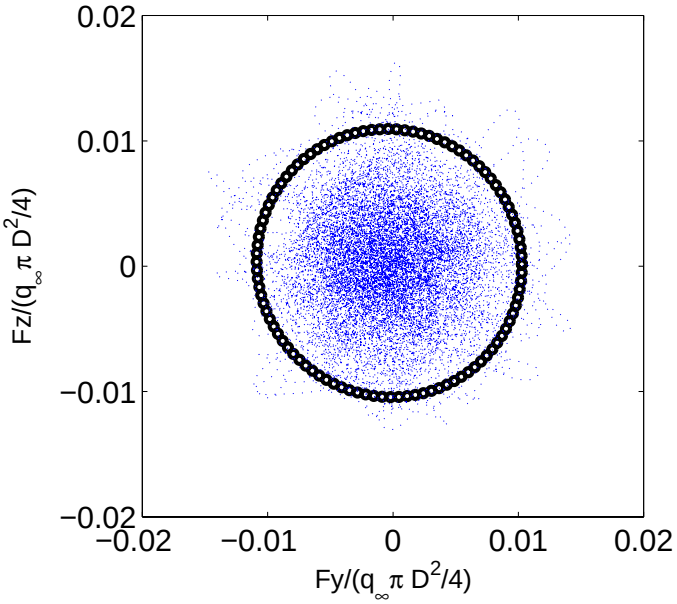

FIG. 12: Polar plot (dotted line) of the computed buffet load and 95% confidence ellipse (symbol)

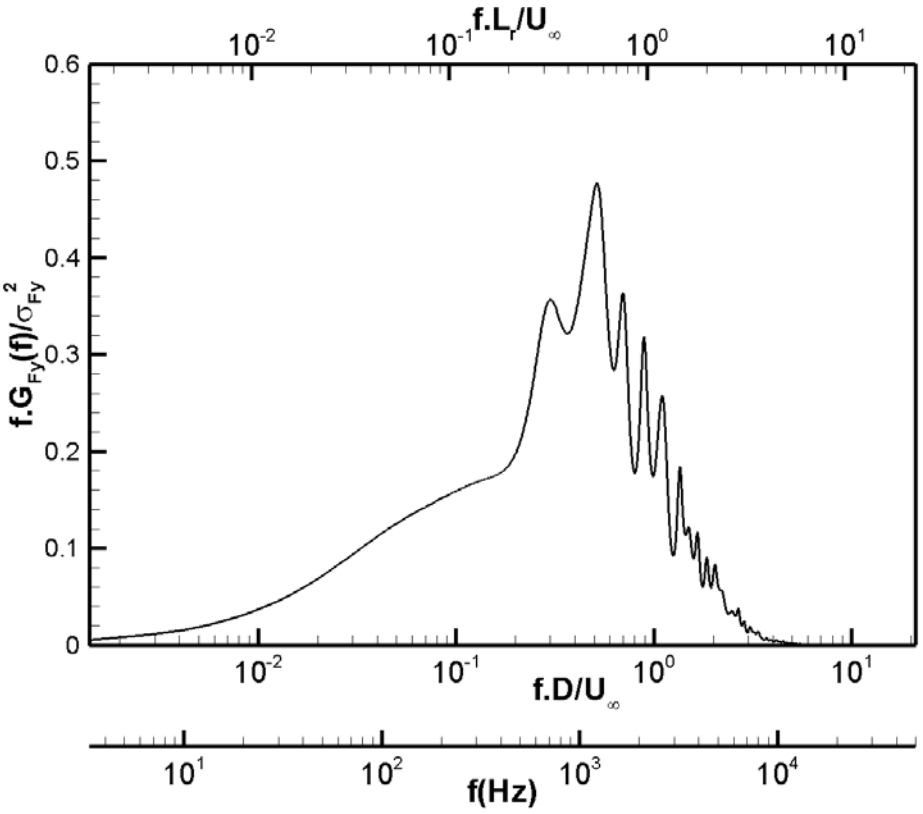

FIG. 13: Spectrum of the Fy buffet load component.

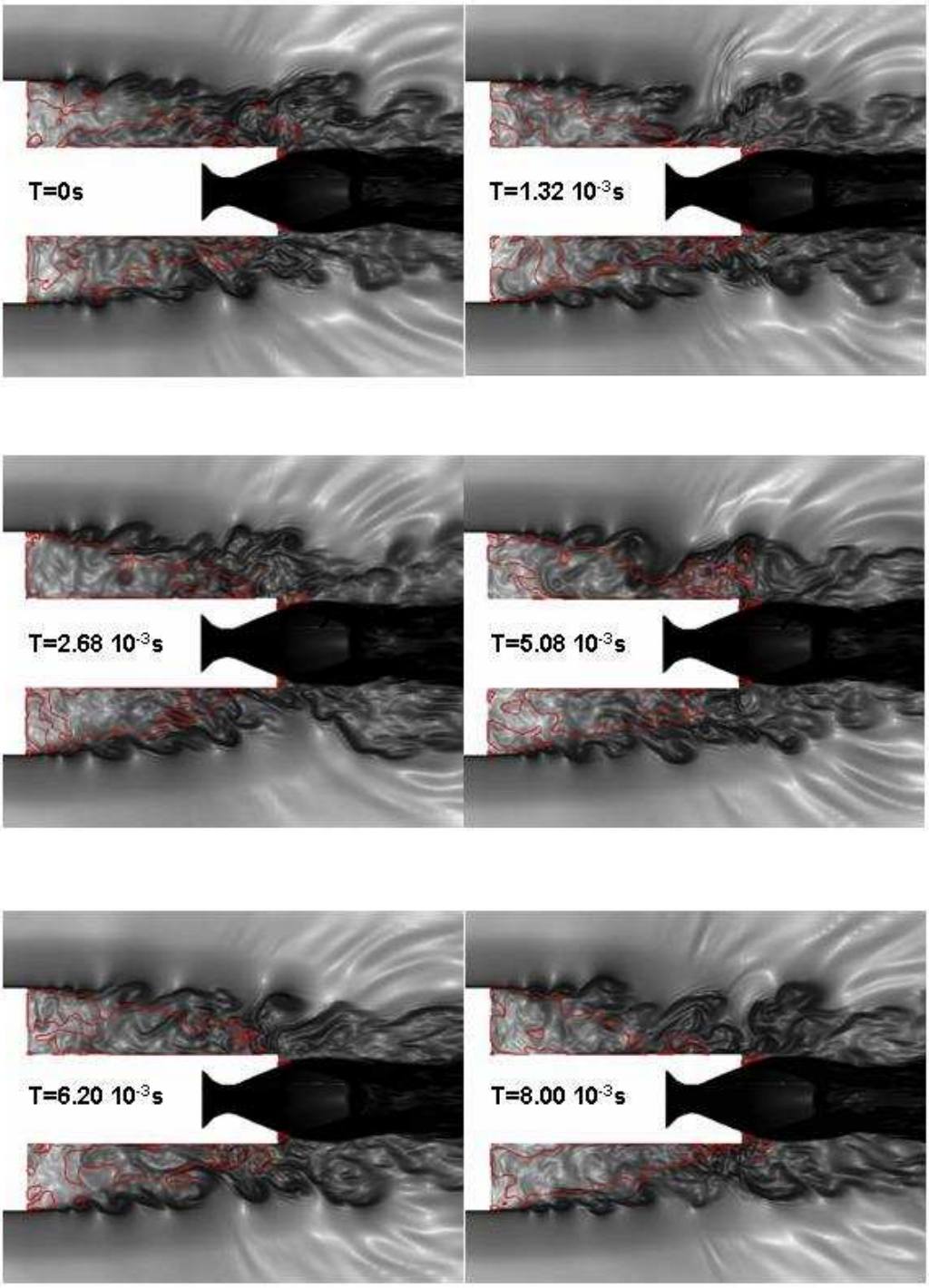

FIG. 14: Numerical snapshots showing the dynamics of the separated region (numerical schlieren).

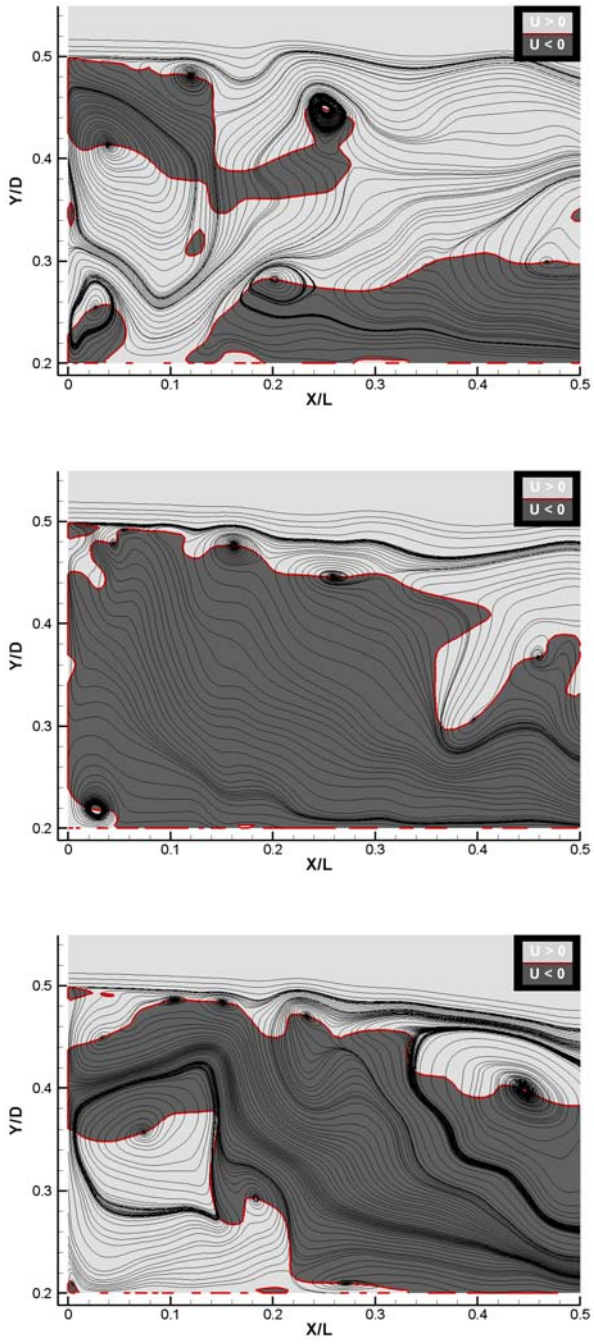

FIG. 15: Corner flow visualization at different times (from top to bottom: times t_0, $t_0 + 2.72\,10^{-3}s$, t_0, $t_0 + 5.4\,10^{-3}s$)

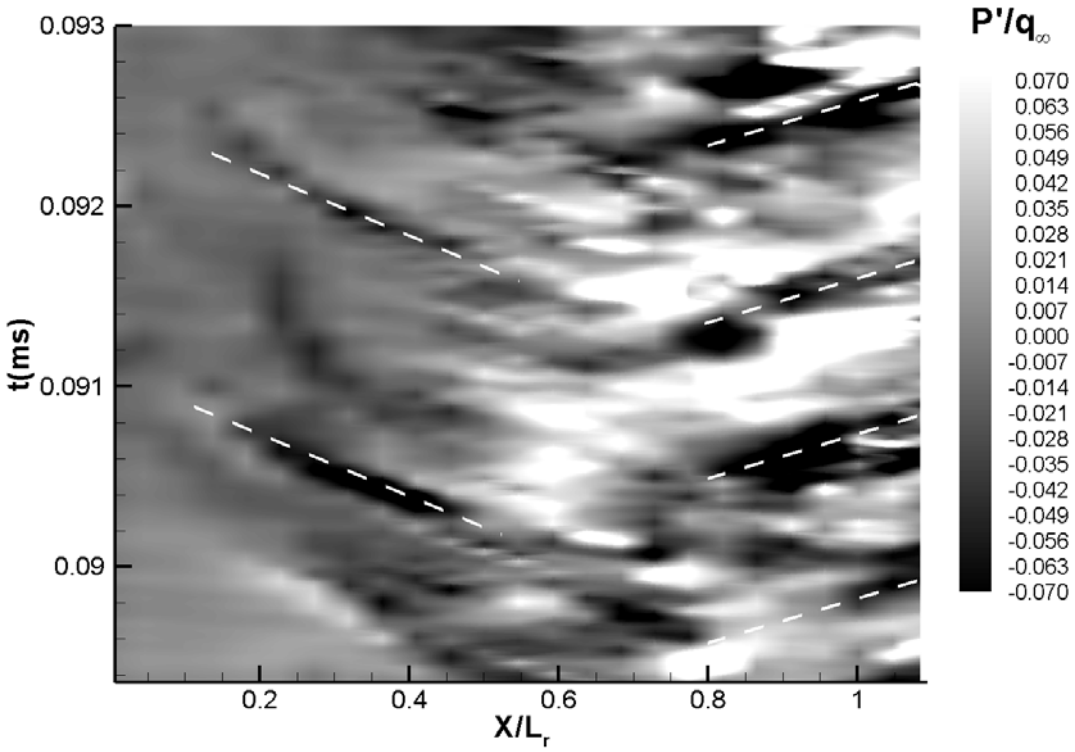

FIG. 16: Space time contours of pressure fluctuations

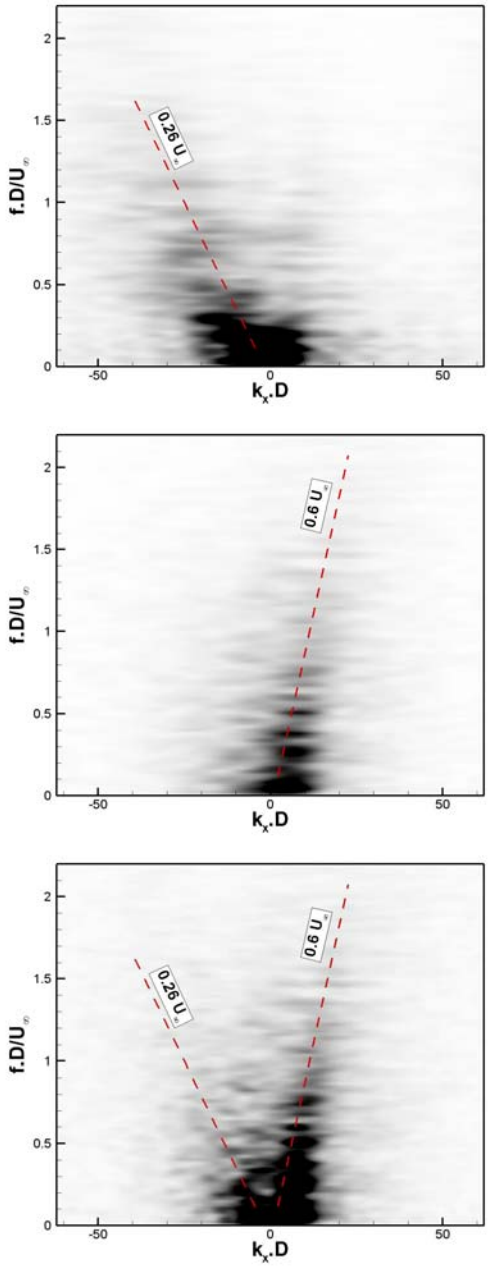

FIG. 17: Frequency-streamwise wave number spectrum. From top to bottom: using points located at $X/L_r < 0.5$ - using points located at $X/L_r > 0.5$ - using all points located in the recirculation bubble.

Tables

Author	**Topology**	M_∞ **or** (U_∞)	Re_D	L_r/D	St_D(dominant frequency)	C_p **base**	**Comments**
Achenbach[82]	sphere	$0.09 m.s^{-1}$	$400 - 5.10^6$	/	$f(Re_D)$	/	vortex separation point rotates around the base
Taneda[11]	sphere	$40 m.s^{-1}$	$10^4 - 10^6$	/	/	/	sphere wake not axisymmetric
Berger *et al.*[12]	sphere	/	$10^4 - 3.10^5$	/	$0.05 - 0.135 - 1.62$ (wake)	/	three kind of instabilities: pumping-shedding-shear layer
Calvert[7]	cone angle $\beta = 0^o - 180^o$	/	5.10^4	1.8	0.246/0.171/0.135 (for $\beta = 0/60/180$)	$-0.24/-0.37/-0.413$ (for $\beta = 0/60/180$)	peak in spectrum only discernable in the wake wake width based Strouhal number $S^* = 0.19$
Eldred[17]	axisymmetric base	$20 - 105 m.s^{-1}$	$2.10^5 - 10^6$	/	≤ 0.1 (wall pressure)	-0.26	Cp_{rms} not constant along the base $0.007 - 0.015$ (highest at the middle of the base)
Merz *et al.*[19,83]	axisymmetric base	$0.11 - 0.94$	$10^6 - 31.10^6$	1.46 at $M_\infty = 0.8$	/	-0.11 for $M_\infty \leq 0.8$	$L_r, C_p, Cp_{rms} \equiv f(M_\infty)$ U_{max} backflow at $X/L_r = 0.6$
Flodrops and Desse[18]	axisymmetric base	$0.43 - 0.85$	$4.7\,10^5$		0.2(wake) 0.06(wall pressure)	-0.1	pressure fluctuations stronger in the middle of the base
Herrin and Dutton[84] Janssen and Dutton[85]	axisymmetric base	2.46	$1.7.10^6$	1.335	0.05 (middle base) 0.095 (edge)	-0.1	$(Cp_{rms})_{max} = 0.006$ at $r/R = 0.56$
Janssen and Dutton[85]	boattailed base	2.46	$1.7.10^6$	/	0.089 (wall)	0.108	$(Cp_{rms})_{max} = 0.005$
Deprés *et al.*[1]	axisymmetric base (L/D=0)	$0.63 - 0.85$	10^6	/	0.08	-0.14	$(Cp_{rms})_{max} = 0.027$ at $r/R = 0$ $Cp_{rms} = 0.014$ at $r/R = 0.7$
Deprés *et al.*[1,41]	L/D=0.6 with and without jet	$0.63 - 0.85$	$1.1\,10^6$ (at $M_\infty = 0.85$)	/ /	0.2 (wall pressure)	-0.13 (no jet) -0.25 (with adapted jet)	$Cp_{rms} = 0.015$ (no jet and $M_\infty = 0.85$) $Cp_{rms} = 0.03$ (with jet)
Lê[53]	axisymmetric base (L/D=0.15)	$0.7 - 0.8$	$7\,10^5$	1.3	0.07	-0.139	$Cp_{rms} = 0.0286$
Lê[53]	L/D=0.55	$0.7 - 0.8$	$7\,10^5$	/	0.2	-0.142	$Cp_{rms} = 0.011$ (no jet and $M_\infty = 0.8$)

TABLE I: Summary of flow data sets featuring a fluidic reattachment (category I). D is the diameter of the axisymmetric body and L stands for the length of an emerging body or splitter plate.

Author	**Topology**	M_∞ **or** (U_∞)	$Re_{D\,or\,H}$	δ/H	L_r/H	Cp_{rms}/q_∞**-max**	**Shedding frequency**	**Flapping frequency**
Simpson[63]	review						$St_{L_r} \approx 0.6...0.8$	$St_{L_r} \leq 0.1$
Mabey[3,29,57]	review					0.04...0.1	$St_{L_r} \approx 0.5...0.8$	
Driver *et al.*[51]	2D BFS	$0.128\,(44 m.s^{-1})$	40000	1.5	6.1	0.04	$St_{L_r} \approx 0.7...0.8$	
Lee and Sung[52]	2D BFS	$10 m.s^{-1}$	$Re_H = 33000$	0.39	7.4	0.034	$St_{L_r} \approx 0.48$	$St_{L_r} \approx 0.1$
Tihon *et al.*[86]	2D BFS	$0.24\,m.s^{-1}$ (water)	$Re_H = 4800$	1	5.1	/	$St_{L_r} \approx 0.65$	$St_{L_r} \approx 0.15$
Hudy *et al.*[54]	2D Fence	$15 m.s^{-1}$	$Re_{2H} = 25600$	0	7.8	0.16	$St_{L_r} \approx 0.7$	$St_{L_r} \approx 0.12$
Cherry *et al.*[45]	2D FPLE	$11 m.s^{-1}$	$Re_H = 32000$	0	4.9	0.125	$St_{L_r} \approx 0.7$	$St_{L_r} \leq 0.125$
Kiya and Sasaki[76]	2D FPLE	$20 m.s^{-1}$	$Re_{2H} = 26000$	0	10	0.12	$St_{L_r} \approx 0.6$	$St_{L_r} \approx 0.12$
Devenport abd Sutton[87]	2D BFS (sudden expansion pipe)	$15 m.s^{-1}$	$Re_H = 35000$	0.2	10.7	/	$St_{L_r} \approx 0.74$	$St_{L_r} \approx 0.16$
Spazzini *et al.*[65]	2D BFS	/	$Re_H = 3500...16000$	/	5...6.5	/	$St_{L_r} \approx 1$	$St_{L_r} \approx 0.08$
Sigurdson[30]	BCC	$12 m.s^{-1}$	$Re_D = 132000 (H/D = 0.25)$	0	7	/	$St_H \approx 0.07$	
Bearman[26]	2D BTE (L/H=3...4)	$14 m.s^{-1}$	$Re_H = 1.45\,10^5$	0.5	2.9	/	no shedding	
Roshko and Thomke[88]	SR	2	$Re_D = 19.10^6 (H/D = 0.14)$	0.54	3.4	/	/	
Mohsen(according to Mabey[57])	2D BFS	0.33	/	$\delta_1/H = 0.5$	4.5	0.06	$St_{L_r} \approx 0.6$	
Coe[55]	SR	0.8	$Re_D = 44.10^6$ $(H/D = 0.167)$	/	5.8	0.06	/	
Kumar *et al.*[56]	SR	0.8	$Re_D = 132200 (H/D = 0.075)$	0.9	7.5	0.05	/	
Deprés *et al.*[1,41]	axi-base (L/D=1.2 and adapted jet)	$0.7\,(237 m.s^{-1})$	$Re_D = 1.1\,10^6 (H/D = 0.3)$	0.7	3.7	0.05	$St_D \approx 0.2$	
Lê[53]	axi-base (L/D=1.22 and adapted jet)	0.7	$Re_D = 7\,10^5 (H/D = 0.285)$	0.18	3.9	0.07	$St_D \approx 0.2$	

TABLE II: Summary of flow data sets featuring a solid reattachment (category II). BFS: backward facing step; SR: step on a body of revolution; FPLE: flat plate leadind edge; BCC: blunt circular cylinder; BTE: blunt trailing edge. δ/H (resp. δ_1/H) denotes the ratio between the incoming boundary layer thickness (resp. displacement thickness) and the step height. D is the diameter of the axisymmetric body and L is the length of an emerging body or splitter plate.

Parameters	**Grid M1**	**Grid M2**	**Grid M3**
$Nx \times Ny \times Nz$	$5.5\,10^6$	$7.0\,10^6$	$8.3\,10^6$
$Nz(\Delta\phi)$	$97(3.75^o)$	$97(3.75^o)$	$147(2.5^o)$
Nx on the emergence (for $0 \leq X \leq L$)	171	221	171
Ny on the base (for $0.2 \leq Y/D \leq 0.5$)	70	85	70

TABLE III: Grid characteristics

Author	**Topology**	$u_{rms}/\Delta u$	$v_{rms}/\Delta u$	$\sqrt{-u'v'}/\Delta u$
Goebel and Dutton[89]	PML	0.220	0.150	0.130
Freund *et al.*[90]	AML	0.195	0.138	0.105
Jovic[49]	BFS	0.200	0.148	0.122
Chandrsuda and Bradshaw[50]	BFS	0.173	0.122	0.105
Castro and Haque[46]	F	0.244	0.244	0.158
present	SR	0.200	0.180	0.141

TABLE IV: Comparison of peak Reynolds stresses in classical shear flows. PML: planar mixing layer; AML: axisymmetric mixing layer; BFS: backward facing step; SR: step on a body of revolution; F: fence flow.